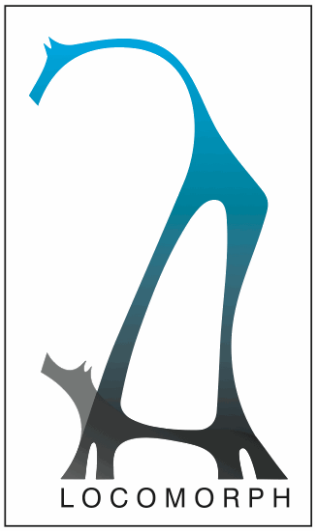

Project no. 231688

LOCOMORPH

Robust Robotic Locomotion and Movements Through Morphology and Morphosis

Small or Medium-Scale Focused Research Project

Seventh Framework Program, Theme: ICT-2007.8.5

Future and Emerging Technologies (FET), Embodied Intelligence

Start date: 1 February 2009 – Duration: 48 months

D4.4 – Simulation and synthesis of movement and gait stability strategies based on verified biomechanical models extracted from experimental results

Due date: 31 July 2012

Actual submission date: 31 July 2012

Number of pages: 4

Project Consortium

Beneficiary no.	Beneficiary name	Short name
1 (Coordinator)	Universitaet Zurich	UZH
2	Friedrich-Schiller-Universitaet Jena	UJEN
3	Ecole Polytechnique Federale de Lausanne	EPFL
4	Syddansk Universitet	USD
5	Universiteit Antwerpen	UANT
6	Ryerson University	RU

Dissemination Level

Project co-funded by the European Commission within the Seventh Framework Programme Dissemination Level		
PU	Public	X
PP	Restricted to other programme participants (including the Commission Services)	
RE	Restricted to a group specified by the consortium (including the Commission Services)	
CO	Confidential, only for members of the consortium (including the Commission Services)	

All Rights Reserved

Contents

This deliverable reports on the simulation and synthesis of movement and gait stability strategies, based on verified biomechanical models extracted from experimental results.
Two approaches are presented. In the first approach, we have started from a very simple mechanical model (SLIP). Only after a profound understanding of its kinematic and kinetic behaviour, complexity (and similarity to the biological system) is increased gradually (M-SLIP, 3D-SLIP).
The second approach starts from a model close resemblance to the biological system and is therefore complex (Webots simulation). From the behaviour of the model under different conditions, general patterns are deduced.
In both modeling approaches, verification with experimental data on animals is performed.

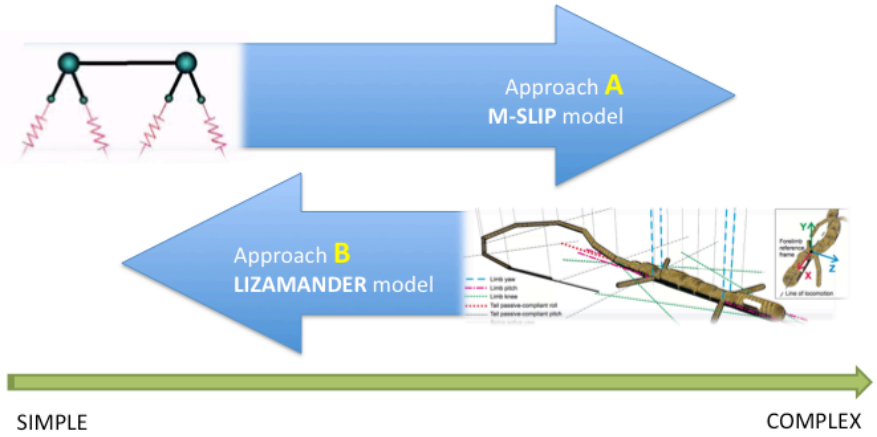

This deliverable consists of the following parts, which are also available publicly on the LocoMorph website http://locomorph.eu/home/project/activities/44:

D4.4.1: Approach A: the M-SLIP model

- D4.4.1.1: **Involuntary morphosis-modular simulation of limb damage in quadrupeds**. (Peuker, Renjewski, Groß, Grimmer and Seyfarth, Proceedings of International Conference Dynamic Walking 2011, Jena, Germany, 2011). We investigate control strategies to stabilize quadrupedal trotting. Afterwards, we identify a strategy to keep the trotting mode while suffering from sudden hind-limb damage.
- D4.4.1.2: **Leg-adjustment strategies for stable running in three dimensions**. (Peuker, Maufroy and Seyfarth, Bioinspir Biomim (2012) vol. 7 (3) pp. 036002). In this journal publication, we show that stability of the 2D SLIP model, which describes human and animal running in sagittal plane, naturally extends to full 3D when the landing angle is defined with respect to velocity. Moreover, all three ground reaction force components of experimental data is in good agreement with predictions of an inherently stable 3D SLIP model solution. We further reveal that the 3D SLIP can inherently stabilize the heading direction and we present a dead-beat similar control to adjust it.
- D4.4.1.3: **Inheritance of SLIP running stability to a single-legged and bipedal model with leg mass and damping**. (Peuker, Seyfarth and Grimmer, BIOROB 2012). In this IEEE publication, we investigate in more detail how leg mass affects model morphology and dynamic behaviour of a running monopod and biped. Including leg mass is necessary to make forward dynamic predictions of the leg's swing phase. We show, that inherent

stability, as previously identified for the 2D SLIP model, is also present and largely preserved by adding leg mass. The suggested control policy is a simple state machine and relies on a serial combination of motor and rotational hip spring. Optimal stiffness and landing angles with respect to energy efficiency are calculated for the applied control scheme.

D4.4.2: Approach B: Simulation and verification of sprawling gait ("Lizamander" locomotion)

- D4.4.2.1: **Locomotion studies and modeling of the long-tailed lizard *Takydromus sexlineatus*.** (Karakasiliotis K, D'Août K, Aerts P and Ijspeert AJ, BIOROB2012). This part reports on the simulation of locomotion in the intact long-tailed lizard, using systematic tests. Input data (morphometrics, performance) from the real animal are used. A good match between the real animal's locomotion, and the simulation is found.
- D4.4.2.2: **Studying morphosis with a simulated model of the long-tailed lizard *Takydromus sexlineatus*: tail amputation**. (Karakasiliotis K, D'Août K, Aerts P and Ijspeert AJ). This part builds on the previous part and extends it in two ways: (1) by addressing the effects of tail morphosis and (2) by using a particle swarm optimization algorhythm. There is good correspondence between how the model and the real animal deal with tail morphosis.
- D4.4.2.3: **Experimental results on locomotion of the long-tailed lizard *Takydromus sexlineatus*: effect of substrate, slope, and tail morphosis**. (D'Août K, Karakasiliotis K, Ijspeert AJ and Aerts P). This part analyses spatio-temporal gait characteristics under a range of conditons (tail morphosis, substrate type and slope) in the long-tailed lizard. Significant differences are found between several combinations of conditions (e.g. different combinations of stride length and frequency to achieve a specific speed) but are overall subtle.
- D4.4.2.4: **Kinematics in healthy and morphosed long-tailed lizards (*Takydromus sexlineatus*): comparison of a simulation model with experimental animal data**. (D'Août K, Karakasiliotis K, Ijspeert AJ & Aerts P). This part specifically tests whether the key findings from the simulation (D4.4.2.2) are also observed in animal experiments. This is overall the case and the simulation model is therefore considered valid.

D4.4.3: Videos

Video footage of this deliverable can be found on the LocoMorph website:
http://locomorph.eu/home/project/activities/44

D4.4.1.1

Involuntary morphosis - modular simulation of limb damage in quadrupeds

Frank Peuker, Daniel Renjewski, Martin Groß, Sten Grimmer and André Seyfarth
Lauflabor Locomotion Laboratory, University of Jena, Dornburger Str. 23, D-07743 Jena, Germany
frank.peuker@uni-jena.de, andre.seyfarth@uni-jena.de

1 Introduction

The ability of humans and animals to adjust posture (voluntary morphosis) increases the versatility of locomotion. It allows a better adaptation to a changing environment. Humans, for example, use bipedalism routinely for efficient and fast locomotion. When they enter rough terrain, get older or carry heavy loads, they may use a walking stick to enhance stability and distribute load. From equally interest is functional and postural adaptation to an unintended structural modification (involuntary morphosis) as caused for instance by limb damage. While humans usually use crutches to restore walking ability, quadrupeds can still locomote with only three operative legs at hand. Applying morphosis strategies in robotics could greatly enhance the adaptability of a legged vehicle: An autonomous robot that can morph could cope with limb damage (e.g. during extraterrestrial missions) and could adapt gait and body morphology to different environments.

To investigate how limb damage affects locomotor ability, we introduce the concept of the bipedal unit (BU). The BU consists of a trunk segment with two attached legs. The simulation model of a BU is based on biologically inspired locomotion templates like the spring-loaded inverted pendulum (SLIP) describing the individual leg function. By combining BUs, quadrupeds and multiple-legged systems can be easily described. This kind of modularity is inspired from robotics as a well-established concept to simplify robot design and to understand robot behavior. However, the BU concept is only one singular realization of modularity in computer simulation and could be considered as a first step towards a sophisticated construction kit for simulating and designing legged robots.

In our presentation, we focus on the question how morphosis in a quadruped can be used to cope with limb damage in order to restore the ability for walking or running.

2 State of the art

The concept of modularity was successfully applied to different legged robots, e.g. Odin [17], RoomBots [16] and salamander robot [7, 8]. Especially the salamander robot can be regarded as a direct inspiration for our BU concept due to its clear decomposition into modules along the fore-aft axis. While these robots do not need any external stabilization,

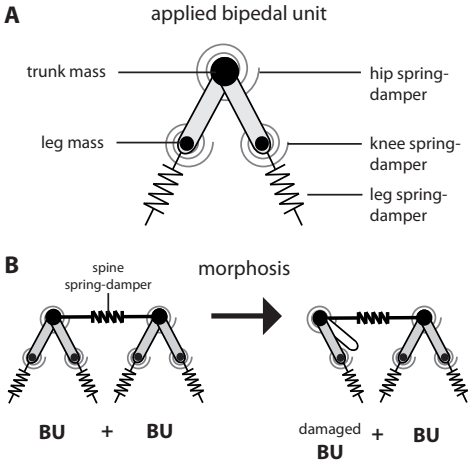

Figure 1: The bipedal unit concept - one realization of modularity in computer simulation. **A.** Our bipedal unit extends the SLIP template by adding leg mass. **B.** Two bipedal units form one quadruped. A hind limb damage causes gait morphosis: Control and morphology is considered for adjustment.

other systems apply lateral, fore-aft or trunk stabilization. This can be achieved, for instance, with a boom mechanism as realized in the GARP robot [15] and JenaWalkerII [14].

The dynamics of human and animal running (e.g. center-of-mass dynamics) are commonly described with simplified models such as the spring-loaded inverted pendulum (SLIP) model [2, 9, 4]. Forward-dynamic simulations of the SLIP model exhibit stable running patterns without the need for actuation (inherent mechanical stability: [3, 6, 11, 13]). This remarkable feature makes the SLIP model a suitable candidate for a running template [5]. By anchoring the SLIP model in more realistic models, the simulation could provide engineers with design requirements as predicted by the model. Thus, robots could be developed that could benefit from inherent stability which relies on energy-efficiency and dynamic stability.

3 Methods

In a simulation study, we adjust leg parameters (e.g. leg and hip stiffness) to compensate for a sudden failure of a quadrupeds hind limb. To assemble the quadrupedal model

we simply connect two BUs with a compliant spine simulated as a prismatic spring-damper element (Fig. 1B). We model the BU in comprising two telescopic springy legs attached to a trunk mass via frictionless hip joints (Fig. 1A). The telescopic leg consists of a leg mass with a linear massless spring underneath. Further, the model has a hip and knee rotational spring-damper element (a linear spring in parallel to a viscous damper). We use actuation of the hip to refill energy that is lost due to leg impact. Hip actuation is achieved by changing the rest position of the hip spring. In fact, our applied BU is an extension of the SLIP model by adding leg masses. With this, dynamic effects of leg rotation (e.g. leg moment of inertia) on running stability can be addressed and torque requirements as well as actuation policies can be investigated in preparation of the robot design. To identify hip actuation policies and model parameters that produce stable running patterns, we use one separate BU and focus on its stability domain. Furthermore, we apply leg retraction strategies [13, 10] to enhance robustness.

4 Discussion outline

To support engineers in robot design, we aim to map the robot together with its environment to a mechanical simulation model. We expect that an iterative, bidirectional transfer between model and robot is beneficial and could yield both models that are modular and robots that are dynamically stable. Within this framework, here, we focused on morphosis strategies that can cope with hind limb damage of a quadruped.

- Which alternative compliant quadrupedal models could be promising?

  Our potential solution: We try to transfer the SLIP as close as possible. This strategy can guide you through high-dimensional parameter and may break the curse of dimensionality [1].

- Which concepts beside *bio-inspiration* could support the construction of dynamically stable legged robots?

  Our potential solution: Using robotic-inspiration for model design could accelerate the bidirectional iteration towards a sophisticated match of model and robot. By identifying underlying structures of this model-robot match, a better understanding of human and animal locomotion would be possible. On the other hand, it would support the development of new design concepts for robots.

- Which additional features beside leg mass could be most important for a sophisticated model-robot match?

  Our potential solution: Adding friction could be beneficial as it was also implemented in the clock-torqued SLIP (CT-SLIP). Robot and CT-SLIP data were in good agreement [12].

References

[1] R. E. Bellman. Adaptive control processes: a guided tour. *Princeton University Press*, page 255, 1961.

[2] R. Blickhan. The spring mass model for running and hopping. *Journal of Biomechanics*, 22(11-12):1217–1227, 1989.

[3] R. Blickhan, A. Seyfarth, H. Geyer, S. Grimmer, H. Wagner, and M. Guenther. Intelligence by mechanics. *Philos T R Soc A*, 365(1850):199–220, 2007.

[4] M. Dickinson, C. Farley, R. Full, M. Koehl, R. Kram, and S. Lehman. How animals move: An integrative view. *Science*, 288:100, 2000.

[5] R. Full and D. Koditschek. Templates and anchors: Neuromechanical hypotheses of legged locomotion on land. *Journal of Experimental Biology*, 202(23):3325–3332, 1999.

[6] S. Grimmer, M. Ernst, M. Gunther, and R. Blickhan. Running on uneven ground: leg adjustment to vertical steps and self-stability. *Journal of Experimental Biology*, 211(18):2989, 2008.

[7] A. Ijspeert. A connectionist central pattern generator for the aquatic and terrestrial gaits of a simulated salamander. *Biological Cybernetics*, 2001.

[8] A. Ijspeert, A. Crespi, and J. Cabelguen. Simulation and robotics studies of salamander locomotion. *Neuroinformatics*, 2005.

[9] T. McMahon and G. Cheng. The mechanics of running: How does stiffness couple with speed? *Journal of Biomechanics*, 23:65, 1990.

[10] F. Peuker and A. Seyfarth. Adjusting legs for stable running in three dimensions. *IFMBE Proceedings. 6th World Congress of Biomechanics, 2010*, Jan 2010.

[11] R. Ringrose. Self-stabilizing running. *PhD*, 1997.

[12] J. Seipel and P. Holmes. A simple model for clock-actuated legged locomotion. *Regular and chaotic dynamics*, 12(5):502–520, 2007.

[13] A. Seyfarth, H. Geyer, M. Günther, and R. Blickhan. A movement criterion for running. *Journal of Biomechanics*, 2002.

[14] A. Seyfarth, F. Iida, R. Tausch, and M. Stelzer. Towards bipedal jogging as a natural result of optimizing walking speed for passively compliant three-segmented legs. *International Journal of Robotics Research*, 2009.

[15] J. A. Smith and J. Jivraj. Preliminary energetics of tripedal and quadrupedal gaits using the garp-4 robot. *Symposium on brain, body and machine*, 2010.

[16] A. Sprowitz, S. Pouya, S. Bonardi, J. Kieboom, R. Moeckel, A. Billard, P. Dillenbourg, and A. J. Ijspeert. Roombots: reconfigurable robots for adaptive furniture. *Computational Intelligence Magazine*, 2010.

[17] K. Stoy, A. Lyder, and R. Garcia. Hierarchical robots. *Proceedings of the IROS Workshop on Self-Reconfigurable Modular Robots, San Diego CA*, 2007.

D4.4.1.2

http://iopscience.iop.org/1748-3190/7/3/036002/

D4.4.1.3

Inheritance of SLIP running stability to a single-legged and bipedal model with leg mass and damping

Frank Peuker, André Seyfarth and Sten Grimmer

Abstract— **Spring-like leg behavior is found in the global dynamics of human and animal running. The corresponding template model, the conservative spring-loaded inverted pendulum (SLIP), shows stability for a large range of speeds and, therefore, is a promising concept for the design of legged robots. However, an anchoring of this template is needed in order to provide functions of biological structures (e.g. mass configuration, leg design) and to provide engineers with detailed guidelines for robot construction. We extend the template model by adding considerable leg mass (M-SLIP) to investigate the influence of leg inertia on running stability. We question whether the model with mass distributed to leg and trunk inherits stable running patterns of the underlying SLIP model. Separately, we investigate single-legged running and alternating bipedal running like humans. Here, we ask for the mass effect of the swing leg on running stability. The results show that the domain of stable SLIP running is anchored in the M-SLIP model. The stability domain is almost completely conserved for bipedal human-like running and reduces slightly for single-legged running. Our study reveals clearly that the SLIP can be anchored in a leg mass model with minimal control effort in using simple hip actuation policies. Our model enhances the theoretical foundation of biologically inspired robotic systems and is a promising candidate for nature-inspired engineering.**

I. INTRODUCTION

The biomechanical description of human and animal locomotion relies on so called template models [1]. A template model is the simplest model with the least number of parameters to describe the basic behavior of the selected gait. The most common template model for human running is the energy conserving spring-loaded inverted pendulum (SLIP, [2]). By abstracting the leg to a massless linear spring with stiffness k and the body to a point mass m, the SLIP is able to resemble the global dynamics[1] of human running in the sagittal plane [2] without any need to provide energy. Furthermore, self-stability[2] is found for the SLIP model if leg stiffness and leg landing angle are adjusted properly [5], [6]. So despite its great simplicity, the SLIP model can recover from small perturbations (e.g. drop height or initial velocity) without any corrective intervention if leg parameters are selected properly. Therefore, the SLIP model can be regarded as a promising concept for the design of legged robots in combining both, self-stability and energy efficiency.

However, the transfer of the SLIP to a technical device needs an anchoring in more elaborate structures. Due to its template character, the SLIP is missing important structures from a higher level of detail like, for instance, trunk, segmented leg, foot, friction, slipping or leg inertia. Following the concept of templates and anchors [1], a piecewise adding of details to the SLIP model reveals major mechanisms and functions of biological structures, and thus, guide engineers towards nature-inspired robotics.

In the present study, we anchor the SLIP model by adding leg mass (M-SLIP, see Fig. 1). About one third of the human mass is due to the legs with the leg CoM located proximally at 40% of leg length [7], [8]. This generates high moments of inertia that can be expected to have significant impact on the overall dynamics. Important effects emerging from our M-SLIP model are for instance swing leg dynamics (in the SLIP model leg dynamics are absent during swing phase) and impact forces caused by the mass-attached leg hitting ground [9]. We also add damping to the model to control leg adjustment during swing phase and to construct a mass-attached telescopic leg that needs no collision model. We use the common concept of hip actuation (e.g. [10], [11], [12]) to compensate energy losses.

We investigate two different kinds of M-SLIP running models, namely single-legged running (1L) and alternating bipedal running like humans (2L). In the SLIP model, both kinds of running coincide since rotation of massless legs is not affecting the runners dynamics. In contrast, in the M-SLIP model we are expecting a significant difference between 1L and 2L running since both mass-attached legs are now coupled and interact continuously. For SLIP running, it was shown that running stability is largely influenced by swing leg protocols [13]. The application of such protocols on mass-attached legs was shown to have several benefits [14] but the influence on the stability domain with respect to leg parameters is yet unclear.

With our novel approach, we aim at investigating the influence of leg mass on SLIP running stability and test the hypothesis that solutions of the simpler SLIP model can be anchored in the more complex M-SLIP model. If so, the curse of dimensionality [15] could be broken. Model designers could now follow the low-dimensional SLIP path of stability within the higher-dimensional M-SLIP solution space to reveal stable gait patterns. To identify stable running patterns, we scan the parameter space with respect to leg stiffness and leg angle while keeping initial velocity fixed. The stability domain, i.e. all combinations of leg stiffness and leg angle that lead to stable running, is known from SLIP simulations [6]. Here, we investigate how this domain is transformed in the M-SLIP model for 1L and 2L running.

All authors are with Sportbiomechanik, Institut für Sportwissenschaft, Technische Universität Darmstadt, 64289 Darmstadt, Germany. peuker@sport.tu-darmstadt.de

[1] i.e. ground reaction force (GRF) and center of mass (CoM) trajectory

[2] For the concept of self-stability cf. [3], [4]

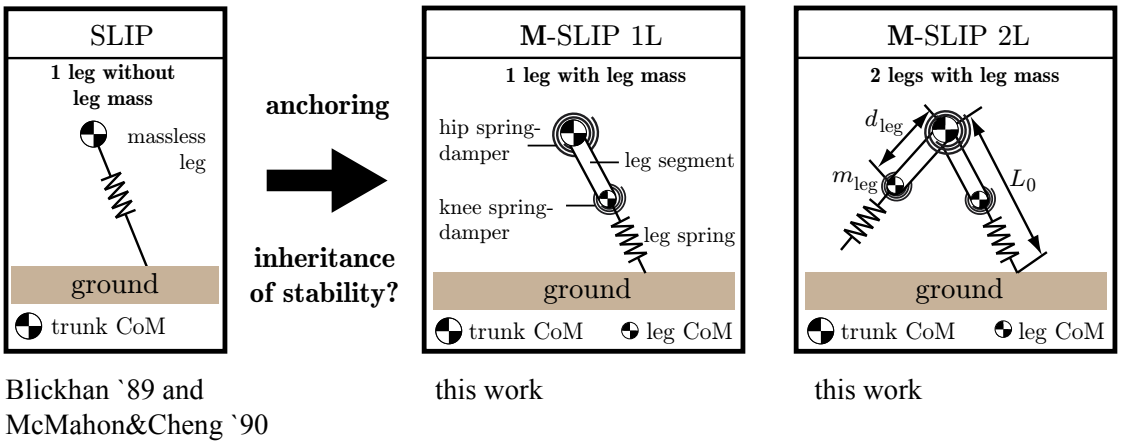

Fig. 1. In this work, we use the M-SLIP model that extends the SLIP model (a template model for human and animal running) by adding leg mass (m_{leg}) at a particular distance from the trunk CoM (d_{leg}). We include a hip spring-damper (parallel combination of linear spring and viscous damper) to control the leg during swing phase and to inject energy during stance phase (according to hip actuation policies A and B, see Fig. 2). We investigate single-legged (1L) and alternating bipedal running (2L) . The knee spring-damper models a telescopic mass-attached leg in aligning leg segment and leg spring.

II. THE SLIP MODEL

Running is described as a succession of stance and flight phases. The SLIP model describes the CoM dynamics (location $\mathbf{r}$) of a runner of mass m with the following equations,

$$m\ddot{\mathbf{r}} = \mathbf{F}_g, \quad \text{in flight phase} \tag{1}$$

$$m\ddot{\mathbf{r}} = \mathbf{F}_g + \mathbf{F}_{\text{leg}}, \quad \text{in stance phase} \tag{2}$$

where $\mathbf{F}_g$ is the gravitational force vector and $\mathbf{F}_{\text{leg}}$ is the force vector of the compressed linear spring acting along leg axis. The value of the leg force is computed with the following relation:

$$|\mathbf{F}_{\text{leg}}| = k_{\text{leg}} \cdot (L_0 - L) \tag{3}$$

Here, L_0 and L denote the nominal and current leg length respectively and k_{leg} is the value of leg stiffness. In the SLIP model, the leg starts in the body CoM and leads into the foot point during stance phase. After instant of lift-off ($L = L_0$) and until next touchdown (flight phase), no leg force is acting. The instant of touchdown and the corresponding foot point is calculated according to the selected leg angle $\alpha(t)$ and nominal leg length L_0. While L_0 is kept constant throughout simulation, we apply the following apex-triggered leg retraction scheme [16] to determine α at time t:

$$\alpha(t) = \alpha_0 + \omega \cdot (t - t_{\text{apex}}) \tag{4}$$

Here, α_0 denotes the initial leg position at instant of apex (t_{apex}) and ω determines the retraction speed. We keep ω fixed at a value of 50 deg/s that was found to be the average in human running [17].

TABLE I

SIMULATION PARAMETERS

parameter	SLIP value	M-SLIP value
nominal leg length L_0	1 m	same
initial speed	5 m/s	same
retraction speed ω	50 m/s	same
total mass M	80 kg	same
leg mass m_{leg}/M	n/a	32% (1L) 16% (2L)
leg CoM d_{leg}/L_0	n/a	40%, proximal
φ_{drive}	n/a	125 deg

III. THE M-SLIP MODEL

A. Model morphology and equations of motion

To account for leg mass in the SLIP model, we add, respectively, one (1L) and two point masses (2L) as shown in Fig. 1. Each leg is mounted to the trunk mass with a frictionless hip joint. Beneath each leg mass, a massless linear spring is attached. We further add one knee and one hip spring-damper per leg (a parallel combination of a rotational linear spring and viscous damper). The application of spring-dampers mimics PD (proportional-derivative) control. We use critical damping to optimally approach a given configuration dynamically ($2 \cdot \text{sqrt}(k_{\text{knee/hip}} \cdot m_{\text{leg}})$). The knee spring-damper is applied to align passively leg segment and leg spring to mimic a telescopic mass-attached leg. The knee-spring damper in combination with the massless leg spring allows a full compliant ground contact. Therefore, no collision model needs to be applied when the leg hits ground and the number of independent coordinates is constant throughout simulation time. The hip spring-damper of each leg, on the other hand, is used for active control and to compensate dissipated energy. To that end, we change the rest angle of the hip spring according to identified hip actuation policies (Fig.2) that are described below. Stiffness of knee (1 kNm/rad) and hip spring (0.75 kNm/rad) are selected from systematic search to minimize

knee bend (telescopic operation) and to allow sufficiently fast leg rotation during swing. The action of knee and hip spring-damper are expressed by torques. Since we use point masses only, these torques are translated to force pairs and are applied to opposing point masses. While the knee spring-damper is an integral part of the body and applies opposing torques to leg spring and leg segment, the hip spring-damper causes only a torque on the corresponding leg segment. Such hip torque could be generated by an external source like a motor mounted on a boom. No collision model is needed in the M-SLIP due to both compliant elements, the telescopic leg spring and the rotational knee spring-damper. The equations of motion are assembled by means of Shabanas embedding algorithm [18]. This algorithm on one hand preserves mass-chain constraints by determining analytical expressions (no constraint violation) and on the other hand allows fast numerical computation by applying a matrix scheme that incorporates the numerical evaluation of intermediate data. The main matrix equation reads:

$$(B^T M B)\ddot{q}_i = B^T Q_e - B^T M \gamma \tag{5}$$

Here, M is the diagonal mass matrix that includes masses of leg and trunk. Any external forces (hip spring-damper, knee spring-damper and leg spring) are accumulated in the external force vector Q_e. The vector q_i includes all generalized coordinates. In 1L running, this vector is of dimension three, including two trunk coordinates and one leg angle. In 2L running, q_i is of dimension four (two leg angles). The both remaining quantities, the velocity-transformation matrix B and the vector γ are determined from the fundamental relationship of generalized coordinates q_i to maximum coordinates q. Whereas the generalized coordinates are independent and already characterize the problem completely, the maximum coordinates are chosen to allow an easy formulation of the external force vector Q_e and to simplify the understanding of the resulting trajectories $q(t)$. In taking the second derivative of the coordinate transformation $q(q_i)$ with respect to time, we can identify B and γ:

$$\ddot{q} = B\ddot{q}_i + \gamma \tag{6}$$

The derivation of (5) and the corresponding quantities B and γ were validated with the symbolic algebra package Mathematica (Wolfram Inc., Champain, IL, USA). Then, the matrices were transferred to MatLab/Simulink (Mathworks Inc., Natick, MA, USA). We use the ode45 integrator (varying time step, fixed order) of MatLab to integrate (1), (2) and (5). The convergence of the numerical formulation was checked by validating the results with a ten times higher accuracy of the integrator.

B. Actuation

We actuate the M-SLIP model by applying different rest angles φ_0 in different states of the gait cycle (see Fig. 1). Thereby, we can achieve both, accounting for energy losses of the passive knee spring-damper (mode 1) and preparing ground contact (mode 2). In 2L running, we need a third mode that accounts for damping of leg rotation only (mode N). The applied actuation policies for 1L and 2L running are shown in Fig. 2. The different modes translate to a rest angle policy in the following manner:

- Mode 1: $\varphi_0 = \varphi_{\text{drive}}$ (constant value, see Tab. 1)
- Mode 2: $\varphi_0 = \alpha_0 + \omega \cdot (t - t_{\text{apex}})$
- Mode N: Leg rotation is damped only.

Mode 1 (applied during stance) injects energy by accelerating leg rotation to a backward position (described with φ_{drive}). Mode 2 initiates the forward swing of the leg by applying SLIP retraction (Eq. 1). We use the same retraction speed of 50 deg/s. In 1L running, we start forward swing immediately after lift off. In 2L running, we delay the forward swing until the contralateral leg touches ground (TDc in Fig. 2). In the meantime (mode N), leg damping prevents physiologically unfeasible leg rotations. 1L and 2L running are applied together with hip actuation policy A and B respectively.

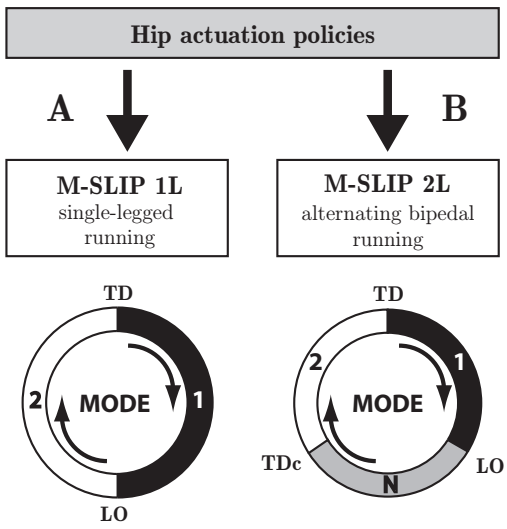

Fig. 2. Hip actuation policies for single-legged running with the M-SLIP 1L model (policy A) and alternating bipedal running with the M-SLIP 2L model (policy B). Policy A switches between mode 1, active during stance phase from touch-down (TD) until lift-off (LO) and mode 2, active otherwise. Policy B is equal to policy A but adds a second mode during flight phase: Between LO and touch-down of the contralateral leg (TDc), mode N is activated. Otherwise mode 2 is used. Different modes correspond to different rest angles of the hip spring-damper: leg retraction (mode 1), energy injection (mode 2), damping of backward leg rotation (mode N) (see text for details).

C. Initial data and simulation parameters

We use physiological data of humans (leg mass, position of leg CoM from [7]). The model is started at apex of CoM trajectory (highest vertical position). The initial apex height of the trunk CoM is set to L_0. The leg that will touch ground first is initially aligned to a rest angle position of α_0. In 2L running we initialize the contralateral leg at a leg angle of $180\ \text{deg} - \alpha_0$.

D. Stable running patterns

We record the number of steps until the model falls over. If the model achieves 50 steps or more, we classify the solution

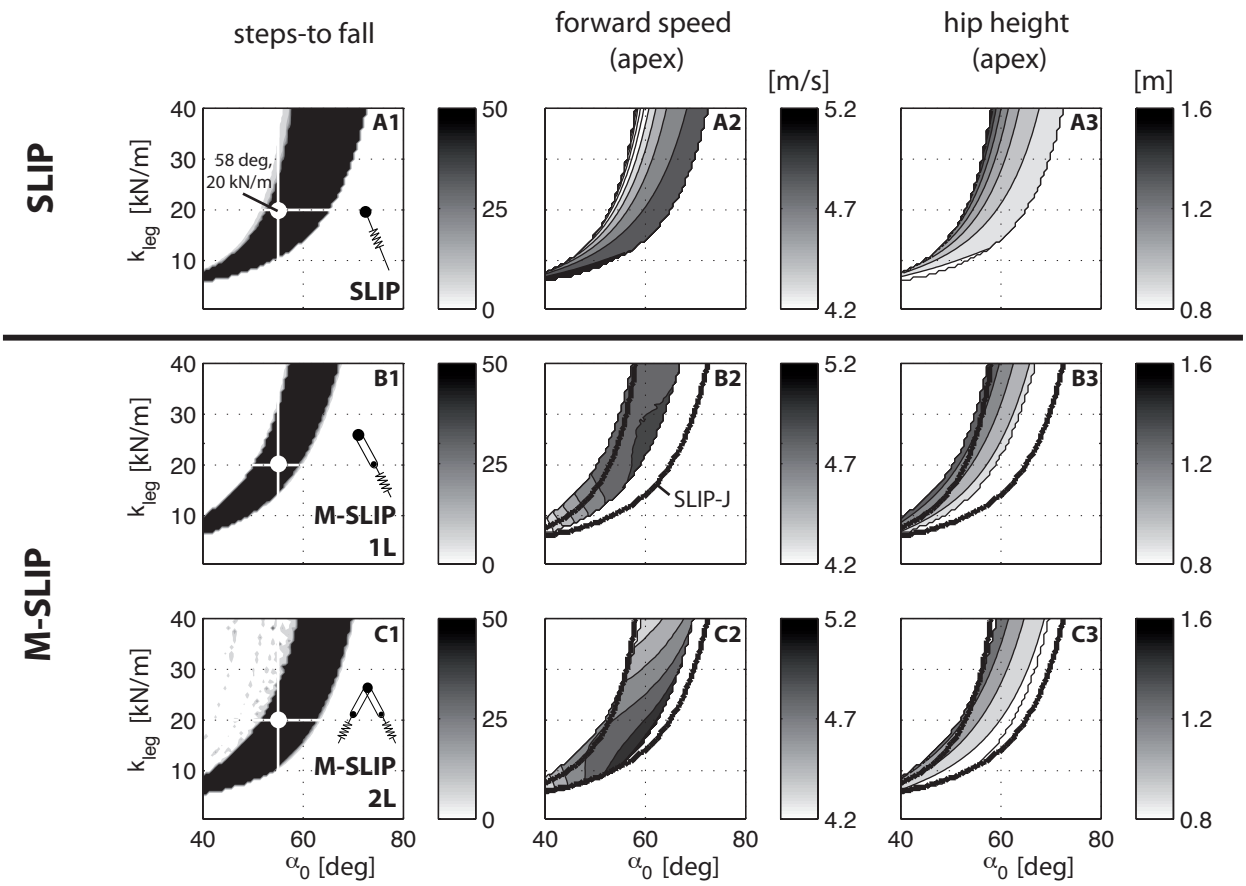

Fig. 3. Steps-to-fall maps by scanning different leg stiffness k_{leg} and leg angles α_0. The domain of stable SLIP running patterns (A1) is anchored in the M-SLIP model for single-legged running (A2) and alternating bipedal running (A3). The stable domains shrink slightly and shift towards flatter α_0 and higher k_{leg}. If stable (accomplishing 50 steps), forward speed (A2-C2) and hip height (A3-C3) is shown. The contour in B2, B3, C2 and C3 shows the original domain of SLIP stability (denoted SLIP-J in B2). For same data type identical scalings of colormaps are used. Physiological leg data from humans are applied ([7]; see Tab. 1).

as *stable* (cf. [6]). We scan different values of leg stiffness k_{leg} and leg angle α_0 on an equidistant grid (64×64) and identify corresponding domains of stable running patterns for the SLIP and the M-SLIP model (see Fig. 3). To compare vertical ground reaction force and CoM excursion of all three models, we select one specific combination (k_{leg} = 20 kN/m, α_0 = 58 deg) and compare corresponding solutions after 50 steps assuming that the model then achieved approximarely steady state.

IV. RESULTS

Steps-to-fall maps of the SLIP (running with massless legs), M-SLIP of single-legged running (1L) and M-SLIP of alternating bipedal running (2L) all show the characteristic J-shape (see Fig. 3). The domain of stable M-SLIP running patterns deforms only slightly with respect to the SLIP model and is reduced in 1L in loosing stability for high leg angles (Fig 3-B2). This holds for 2L as well but the effect is reduced here to a large extent (Fig. 3-C2). On the other hand, stable running patterns are added for small leg angles in 1L and 2L but the additional stability cannot compensate completely for the lost stability if comparing the area of stability domain. At the apex of the CoM (including trunk and leg masses), we recorded hip height (Fig. 3: A3-C3) and CoM forward speed (Fig. 3: A2-C2). With respect to the SLIP (Fig. 3A3), 1L running shows similar hip heights. In 2L running, the hip height is significantly reduced and approaches 0.8m for larger angles of attack (Fig.3-C3). For all three different models (SLIP, M-SLIP 1L and 2L), the isoline collection shows a similar shape allowing the general rule that hip height is higher for larger angles than for smaller angles of attack. The collection of isolines for forward speed, in contrast, reveals a different shape in the M-SLIP models (Fig. 3-B2 and 3-C2) if compared to the SLIP (Fig. 3A2). Highest forward speeds occur at 25 kN/m in 1L and 15 kN/m for 2L running when applying the greatest angle of attack that yield a stable running pattern at the given leg stiffness. The SLIP model, on the other hand, does not show such an optimum inside the recorded domain. We select one pair of leg stiffness k_{leg} = 20 kN/m and leg angle α_0 = 58 deg (tagged with a white dot and a hair cross in Fig. 3: A1-C1) to record vertical ground reaction force (vGRF, Fig. 4A) and CoM excursion (Fig. 4B) of all three models in steady state. The vGRF of all three

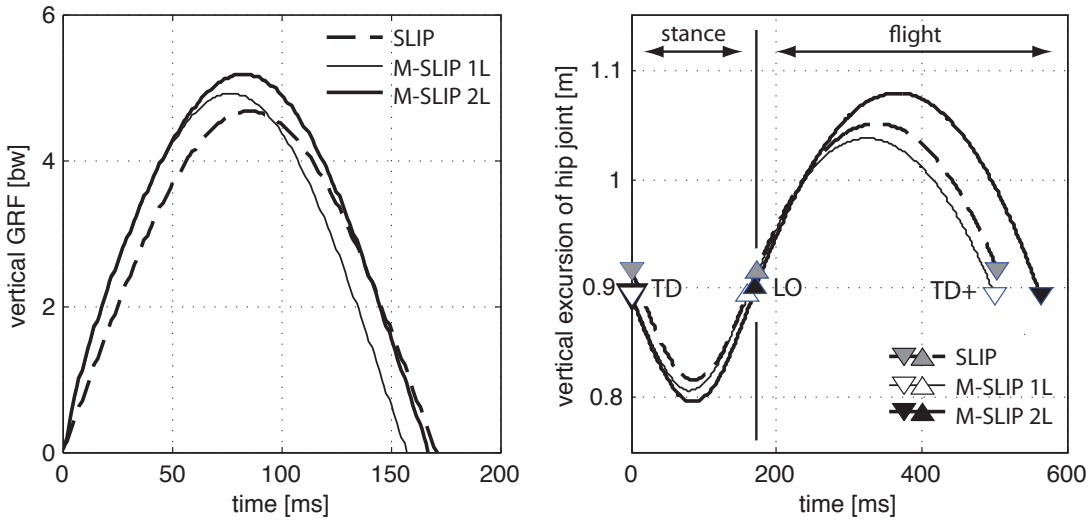

Fig. 4. Comparison of all three models SLIP (dashed line), M-SLIP 1L (medium line) and M-SLIP 2L (thick line) using identical leg parameters k_{leg} = 20 kN/m and α_0 = 58 deg. A. Vertical ground reaction force (vGRF) in body weights (bw) . B. Vertical excursion of the hip joint during one complete gait cycle (stance and flight phase). Triangle markers show touch-down (TD), lift-off (LO) and subsequent touch-down (TD+) of steady state solution.

models reveal a smooth single hump. The peak vGRF is slightly higher and is approached earlier in M-SLIP models compared to the SLIP. The contact time is almost identical for M-SLIP 2L and SLIP whereas it is slightly shorter in the M-SLIP 1L model. Due to the control concept, touch down height is smaller in M-SLIP model (Fig. 4B) since the rest angle is not approached instantly as in the SLIP model. The M-SLIP 1L model exhibits the flattest parable in flight phase, whereas M-SLIP 2L shows the highest.

V. DISCUSSION

In this study, the effect of leg mass on running stability of the SLIP model was investigated by means of the novel M-SLIP model that supports single-legged running (1L) and alternating bipedal running like humans (2L). We asked if stability of the SLIP model is anchored and reproduced in the more complex M-SLIP model. The simulation results show that M-SLIP anchors SLIP stability to a remarkable amount (Fig. 3). Biologically data of humans were used to fix parameters of mass distribution. No fine-tuning or optimization was needed for both, 1L and 2L running.

A. Self-stability of SLIP running patterns is anchored in our M-SLIP model

Successful inheritance of desirable features such as self-stability is the paramount idea behind the concept of templates and anchors [1]. Self-stability is desirable as it describes the feature to recover inherently from perturbations without any need for corrective intervention. With the present work, we showed that self-stability of SLIP running can be anchored in our M-SLIP model. To anchor SLIP self-stability, it was sufficient to select free M-SLIP parameters according to the SLIP model (e.g. adjust knee spring-damper to mimic telescopic leg, use hip spring-damper to control leg angle). Furthermore, the leg parameter domain (k_{leg}, α_0) of stable running patterns as observed in the SLIP model is predominantly reproduced in both M-SLIP models (1L and 2L, Fig. 3). Like in humans [7], we equipped our model with a total leg mass of about one third of the total mass. Surprisingly, the resulting high moments of leg inertia due to leg oscillation (backward and forward swing) had only a minor effect on the stability domain. This suggests that the SLIP model can be naturally anchored in leg-mass models. Interestingly, the domain of stable running patterns shifts slightly to flatter leg angles and higher leg stiffnesses for both 1L and 2L running (see Fig. 3-B2, 3-C2). This effect can be attributed to a decreasing nominal leg length of the underlying SLIP model since leg mass cause the CoM to be below hip in the M-SLIP model. In the SLIP, forward speed is coupled to CoM height due to energy conservation (compare Fig. 3-A2 and 3-A3). In contrast, since energy conservation is abandoned in the M-SLIP models, forward speed changes differently compared to the CoM height when leg parameters are varied (compare Fig. 3-B2 with 3-B3 and 3-C2 with 3-C3 respectively). Surprisingly, this new distribution allows us to identify an optimal leg stiffness in terms of maximal forward speed (1L: $\sim$25 kN/m, 2L: $\sim$15 kN/m). This result is likely due to our particular hip actuation policy and could be further exploited in more elaborate actuation schemes (Fig. 2). In all three models, forward speed is maximal if the leg angle α_0 is selected from the right boundary of the J-shaped stability domain. Vertical ground reaction force (vGRF) and trajectory of the trunk mass show a similar shape for all three models, SLIP, M-SLIP 1L and M-SLIP 2L (Fig. 4). Due to extra

hip torque, M-SLIP vGRF exceeds SLIP vGRF in the first part of stance phase. Interestingly, even though the knee spring-damper could cause an impact peak at touch-down, it was not observed in steady state solutions. This could be due to an inherent adjustment of the M-SLIP model to the underlying SLIP running pattern. The contact time is slightly shorter for 1L running than in 2L running, which can be explained with the backward-oriented action of the leg torque that cause the vertical ground reaction force to drop to zero earlier. Consequently, such effect is not present in 2L running where both legs act in an alternating manner (M-SLIP 2L). Alternate running can produce the flattest trajectories as indicated by hip height for steep leg angles α_0 (Fig. 3-C3). However, this important insight is not reflected in Fig. 4 since we used fixed leg parameters for comparison. Due to this constraint, the leg angle for M-SLIP 2L running could not be selected from the right boundary of the stability domain where flat trajectories are predominant (Fig. 3-C3).

B. Properties and limitations of the M-SLIP model

Impact peaks can only originate from the knee spring-damper in the M-SLIP model, whereas they can also come from direct collisions of the foot with ground for both barefoot running [19] and rearfoot running [20]. Such features are not yet incorporated in the M-SLIP model. Furthermore, the M-SLIP model neglects the problem of trunk stabilization and thus is mimicking the idea to fix the robot on a boom (e.g. SLIP hopper [21], Jena-Walker [22], GARP [23]).

VI. CONCLUSIONS

In this work, we anchored the SLIP model by adding leg masses and damping (M-SLIP). We reproduced SLIP stability domains in the M-SLIP model for single-legged and alternating bipedal running. The domain of leg parameters that lead to self-stable running patterns is predominantly conserved. Vertical ground reaction forces and CoM trajectories deviate only slightly from the simpler SLIP model. The results are promising and supporting the idea that realistic and complex models can be derived from simplistic templates that feature benefits like self-stability. As a result, we suggest to break the curse of dimensionality that dominates complex models by adjusting new degrees of freedom to mimic closely the SLIP model. This strategy could pave the way for realistic models that guide engineers towards dynamically running humanoid robots.

VII. ACKNOWLEDGMENTS

The research leading to these results has received funding from the European Communitys Seventh Framework Programme FP7/2007-2013 - Future Emerging Technologies, Embodied Intelligence, under grant agreement no. 231688. The author further thanks Rico Möckel and Soha Pouya from EPFL as well as Martin Groß and Sebastian Riese for helpful advice and discussions.

REFERENCES

[1] R. Full and D. Koditschek, "Templates and anchors: Neuromechanical hypotheses of legged locomotion on land," *The Journal of Experimental Biology*, vol. 202, no. 23, pp. 3325–3332, 1999.

[2] R. Blickhan, "The spring-mass model for running and hopping," *Journal of biomechanics*, vol. 22, no. 11-12, pp. 1217–1227, 1989.

[3] S. Grimmer, M. Ernst, M. Günther, and R. Blickhan, "Running on uneven ground: leg adjustment to vertical steps and self-stability." *The Journal of Experimental Biology*, vol. 211, no. Pt 18, pp. 2989–3000, Sep. 2008.

[4] R. Ringrose, "Self-stabilizing running," in *Robotics and Automation, 1997. Proceedings., 1997 IEEE International Conference on*, 1997, pp. 487–493.

[5] H. Geyer, A. Seyfarth, and R. Blickhan, "Compliant leg behaviour explains basic dynamics of walking and running," *Proceedings Biological sciences / The Royal Society*, vol. 273, no. 1603, pp. 2861–2867, Nov. 2006.

[6] A. Seyfarth, H. Geyer, M. Günther, and R. Blickhan, "A movement criterion for running," *Journal of biomechanics*, vol. 35, no. 5, pp. 649–655, May 2002.

[7] C. Clauser, "Weight, volume, and center of mass of segments of the human body," DTIC Document, Tech. Rep., 1969.

[8] C. E. Clauser, J. T. McConville, and J. W. Young, "Weight, Volume, and Center of Mass Segments of the Human Body," *Journal of Occupational and Environmental Medicine*, vol. 13, no. 5, p. 270, May 1971.

[9] A. Seyfarth, A. Friedrichs, V. Wank, and R. Blickhan, "Dynamics of the long jump," *Journal of Biomechanics*, vol. 32, no. 12, pp. 1259–1267, Dec. 1999.

[10] M. M. Ankarali and U. Saranli, "Stride-to-stride energy regulation for robust self-stability of a torque-actuated dissipative spring-mass hopper," *Chaos*, vol. 20, no. 3, p. 033121, 2010.

[11] J. Seipel and P. Holmes, "A simple model for clock-actuated legged locomotion," *Regular and chaotic dynamics*, vol. 12, no. 5, pp. 502–520, 2007.

[12] B. S. Andrews, B. Miller, J. Schmitt, and J. Clark, "Running over unknown rough terrain with a one-legged planar robot," *Bioinspiration & biomimetics*, vol. 6, no. 2, p. 026009, 2011.

[13] H. Knuesel, H. Geyer, and A. Seyfarth, "Influence of swing leg movement on running stability," *Human Movement Science*, vol. 24, no. 4, pp. 532–543, Aug. 2005.

[14] M. Haberland, J. Karssen, S. Kim, and M. Wisse, "The effect of swing leg retraction on running energy efficiency," in *Intelligent Robots and Systems, 2011. Proceedings., 2011 IEEE International Conference on*. IEEE, 2011, pp. 3957–3962.

[15] R. Bellman, *Adaptive control processes: a guided tour Princeton University Press*. Princeton, 1961.

[16] A. Seyfarth, H. Geyer, and H. Herr, "Swing-leg retraction: a simple control model for stable running," *The Journal of Experimental Biology*, vol. 206, no. Pt 15, pp. 2547–2555, Aug. 2003.

[17] Y. Blum, S. W. Lipfert, J. Rummel, and A. Seyfarth, "Swing leg control in human running," *Bioinspiration & biomimetics*, vol. 5, no. 2, p. 026006, 2010.

[18] A. A. Shabana, *Computational Dynamics*, 3rd ed. Wiley, Mar. 2010.

[19] D. E. Lieberman, M. Venkadesan, W. A. Werbel, A. I. Daoud, S. D'Andrea, I. S. Davis, R. O. Mang'eni, and Y. Pitsiladis, "Foot strike patterns and collision forces in habitually barefoot versus shod runners." *Nature*, vol. 463, no. 7280, pp. 531–535, Jan. 2010.

[20] T. Novacheck, "The biomechanics of running," *Gait and Posture*, vol. 7, no. 1, pp. 77–95, 1998.

[21] A. Sato and M. Buehler, "A planar hopping robot with one actuator: design, simulation, and experimental results," *Intelligent Robots and Systems, 2004.(IROS 2004). Proceedings. 2004 IEEE/RSJ International Conference on*, vol. 4, pp. 3540–3545 vol. 4, 2004.

[22] K. Kalveram, D. Haeufle, and A. Seyfarth, "From hopping to walking. how the biped jena-walker can learn from the single-leg marco-hopper," in *Advances in Mobile Robots. Proceedings of the 11th International Conference on Climbing and Walking Robots (CLAWAR).*, 2008, pp. 638–645.

[23] J. Jivraj and J. Smith, "Primary energetics analysis of tripedal and quadrupedal gaits using the garp-4 robot," in *Electrical and Computer Engineering (CCECE), 2011 24th Canadian Conference on*. IEEE, 2011, pp. 001 206–001 211.

D4.4.2.1

Locomotion studies and modeling of the long-tailed lizard Takydromus sexlineatus

Konstantinos Karakasiliotis*, Kristiaan D'Août, Peter Aerts and Auke Jan Ijspeert, *Member, IEEE*

***Abstract*— Morphology is an important factor in locomotion. It may guide the control strategies that an animal or a robot uses for efficient locomotion. In this paper we try to understand the locomotion strategies of a lizard with a distinctive feature, the long-tailed lizard Takydromus sexlineatus. We recorded the performance of real animals in terms of forward speed and then developed a simulation model respecting the morphometric characteristics of long-tailed lizards. We then run systematic tests altering several control parameters of the model. The simulation experiments suggested possible control strategies for effective locomotion given this type of morphology. The experiments were not constrained or guided by any prior knowledge on specific animal angular kinematics. Therefore, the good match between the suggested kinematics for optimal speed and the kinematics of the real animal suggests that our framework is capable of exploring in the future the effects of morphosis on the locomotion strategies of animals, i.e. to perform the same study with shorter or no tail.**

I. INTRODUCTION

When it comes to fast, stable and adaptive locomotion, lizards are one of the best animal groups to study. Moreover, lizards display a wide range of morphological diversity and ecological adaptations, including the ability to locomote on a variety of substrates ([1]). Lizard locomotor mechanics are remarkably similar to those of other legged animals ([2]) which suggests that similar locomotor strategies might be shared with other tetrapod groups. Understanding how specific morphological variations affect the locomotion strategies of animals may reveal the principles that connect morphology and control.

Within the lizard taxon (Lacertilia), in the family of Lacertidae all members are relatively closely related. This increases the chances that observed morphological diversity within this family reflects functional diversity, and not phylogenetic diversity.

Within the Lacertidae, two species, the Lacerta vivipara and Takydromus sexlineatus have similar body size and they display a general "lizard" body shape, i.e. with not extremely strong developed (as is specialist runners) or underdeveloped (as in scincids) limbs. The specialist, T. sexlineatus, differs from the generalist L. vivipara mainly in one, clear, distinguishing feature: extreme tail elongation ([3] – [5]). This should facilitate interpretation of biomechanical comparisons between these species. Lacerta is the generalist reference, and a considerable amount of literature is available on general characteristics of lizard locomotion ([2], [6], [7]).

Konstantinos Karakasiliotis and Auke Jan Ijspeert are with the École Polytechnique Fédérale de Lausanne (EPFL), Switzerland.

Kristiaan D'Août and Peter Aerts are with the Laboratory for Functional Morphology, Department of Biology, University of Antwerp, Belgium.

Fig. 1. Snapshot of the long-tailed lizard during the experiments.

Therefore, the main focus of our study is on Takydromus (Fig. 1) because it sports a clear case (tail elongation) of long-term morphosis. In particular, we address two basic questions: i) What are the control parameters for which the model closely replicates the basic kinematics of the long-tailed lizard? and ii) What body postures can optimize the model's performance in terms of speed and how do they compare to the real animal? It is important here to note that these questions were not guided by kinematic recordings from the specific animal and, therefore, the optimal solutions from our systematic exploration of control parameters was only dependent on the specific morphological and inertial properties of the model.

II. LONG–TAILED LIZARD KINEMATICS

A. Materials and Methods

For the animal experiments, 15 Takydromus sexlineatus were acquired commercially and housed in a terrarium with plenty of food and water, and the possibility to thermoregulate. Average body mass was 3.80 ± 0.73 g (range: 2.47 – 5.12 g), average total body length was 304 ± 32 mm (range: 225 - 358 mm), and the percentage of total body length that is tail was $82 \pm 2\%$ (range: 75 – 85%), i.e. the tail is 3 to 5.6 times longer than snout-vent length.

Animals were filmed dorsally using a high-speed digital video camera (300 fps, Casio EX-F1). Subsequently, anatomical landmarks were digitized manually, frame-by-frame, and used for conventional gait assessment (spatiotemporal gait variables, speed and frequency).

After kinematic experiments, one individual was sacrificed, frozen in a straight position and segmented using a sharp scalpel. Frozen body segments were weighed on a Mettler microbalance. The following segments were measured: head, neck, trunk (in five segments of equal length), tail (in ten segments of equal length), upper leg, lower leg and foot (Fig. 2). For each segment, mass, length, and average width (for trunk and tail segments) was measured. These measurements were used then to define the inertial properties of the simulated model (see section III-A and

TABLE I

MORPHOMETRICS OF THE LONG-TAILED LIZARD

Body part	Length (mm)	Width (mm)	Mass (mg)
head	13.86	-	311.4
neck	4.66	-	105.25
trunk A	7.558	5.84	241.09
trunk B	7.558	6.4	294.57
trunk C	7.558	7.19	315.37
trunk D	7.558	7.91	218.11
trunk E	7.558	5.63	284.66
tail A	26.591	5.535	379.36
tail B	26.591	3.795	227.71
tail C	26.591	3.495	190.49
tail D	26.591	3.265	153.65
tail E	26.591	3.04	125.84
tail F	26.591	2.855	95.35
tail G	26.591	2.565	74.16
tail H	26.591	2.2	49.87
tail I	26.591	1.7	24.77
tail J	26.591	0.985	6.76
upper leg	7.49	-	31.99
foreleg	7.27	-	22.16
foot C	14.68	-	14.53

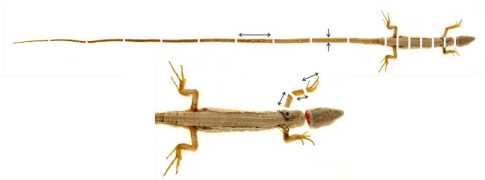

Fig. 2. Morphometrics of Takydromus sexlineatus. On top, the head, neck, trunk (in five segments of equal length) and tail (in ten segments of equal length) are illustrated along the full length of the animal. At the bottom, a closed view shows the segmentation of the upper leg, lower leg and foot.

Table I). All animal experiments have been approved by the Ethical Committee for Animal Experiments of the University of Antwerp (19/12/2008, file 2008-34).

B. Results

Typically, lizards move using walking and trotting gaits employing a sprawling posture with the limbs extended laterally. Their elongated body is moving laterally on either side of their line of locomotion using a form of standing wave. This wave can have 2 or more nodes where its lateral movement changes direction. For the long-tailed lizard two of the nodes are found around the regions where the front and hind limbs are attached to the body. The rest of the nodes are on the tail. However, these are not consistent either in number or in position indicating that passive properties and the length of the tail complicate its function. Possibly, on a smooth floor, the tail is mainly dragged.

Spatiotemporal recordings of the long-tailed lizards showed a wide range of locomotion frequencies (3.5 – 8.5 Hz) and forward speed (0.14 – 0.6 m/s). Fig. 3 shows these results for $N = 15$ individuals (filled circles). The red line corresponds to the linear regression of the data points. In this plot it is clear that frequency is increasing with speed and the two variables are highly correlated with a positive correlation coefficient at around 90%. This indicates that one definite strategy for the long-tailed lizard for faster

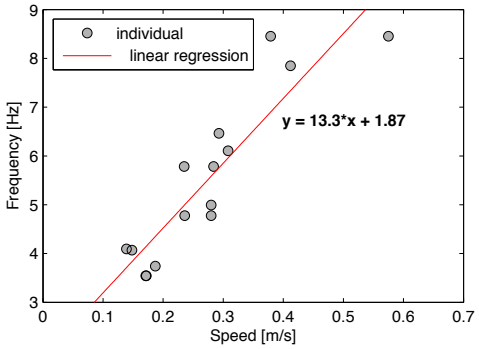

Fig. 3. Kinematic results from the long-tailed lizard experiments. The plot shows the relationship between locomotion frequency and forward speed for each individual(filled circles). The red line corresponds to the linear regression of the data points and its equation is shown in bold. Speed is highly correlated to the frequency of locomotion (correlation coefficient = 90.5%).

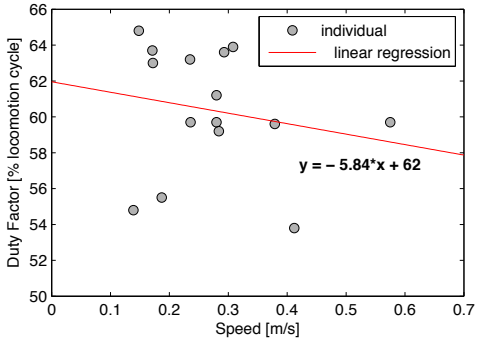

Fig. 4. Relationship between the forward speed and the duty factor of the hind limbs. Conventions here are the same as in Fig. 3. The correlation coefficient is −19.4%.

locomotion is to increase its frequency of locomotion. In our experiments, all the individuals employed a type of gait that can be classified as a walking trot ([8]) where two diagonal limbs are in phase with each other and in anti-phase with the resting pair. The difference with a typical trot is that, here, a short overlap can occur between the stance phases of the contralateral limbs and three feet can be touching the ground simultaneously. This can happen when the duty factor is greater than 50%. Duty factor is the ratio between the stance period of a particular limb over the total period of the locomotion's cycle. Fig. 4 shows that all the recorded duty factors of the hind limbs of the lizards were greater than 50%. This happens for all the range of speeds (and frequencies) with a low negative correlation of $\approx -20\%$. The negative sign of the correlation, however, denotes that the duty factor tends to (slowly) decay for higher speeds or frequencies.

III. MODELING LONG–TAILED LIZARD LOCOMOTION

A. The long-tailed lizard model

We developed a model of the long-tailed lizard in the ODE-based simulation platform Webots™. The segmentation, geometry and inertial properties of the model are based

on the lizard's morphometric measurements as shown in Table I.

One of the features of sprawling locomotion is the movement, mainly, on the horizontal plane. Therefore, the spine of the lizard model is composed of 16 vertical active degrees of freedom (DoF) positioned according to the segmentation of the example animal in Fig. 2. Additionally, 5 passive compliant DoF were added to the tail of which 4 enable vertical movements and the last one rolling movements along the body-axis (Fig. 5). It is important to enable rolling of the tail at the point where the trunk ends in order to decouple rolling movements of the main body from the lengthy plane of the tail. The latter, along with the segmentation of the limbs, significantly improved the stability of our model. The compliance of the passive DoF is implemented as a simple spring and damper. The distribution of these passive DoF along the tail, as well as the coefficients for the springs and dampers, had been decided through manual experimentation aiming at, as much as possible, a more natural behavior.

Each limb is composed of 3 active DoF and implemented as a pitch-yaw-knee manipulator. The pitch moves the limb vertically (adduction-abduction), the yaw, horizontally, back and forth (retraction-protraction) and the knee extends and retracts the foreleg. We did not implement a palm segment in order to avoid additional complexity for the control (due its complex and adaptive behavior) and because, from observation, the palm of the animal is mainly kept on the ground throughout the stance phase mainly acting as a friction pad. Note that a more precise model of the limbs would be to add a roll DoF at the shoulders/hips. Although this would lead to more natural limb postures, the inclusion of such a DoF would add complexity to the control without any significant advantage for the locomotion studies. This is because, as we will see in section III-B, our control is based on the cartesian trajectory of the feet where one can prove that both limb configurations (with or without roll) have the same reachable space.

The ground contact model is based on the ODE's contact model which is implemented as a spring and damper between the colliding objects. This behavior resembles the soft tissues of the animal's feet or any other natural compliance between the animal and the ground. Our model did not show major sensitivity to different values of these parameters and no high damping was needed for the model to be stable as soon as the kinematics where optimized and well coordinated.

B. Control

We use position control for all active DoF of the model with relatively high PID gains. This ensures that the defined postures and trajectories are respected, even in high frequencies.

1) Spine: The spine is controlled by a simple sine controller. The angle of each active DoF, θ, is given by:

$$\begin{aligned} \theta_i &= A_i sin(\phi + \psi_i), \quad 1 \leq i \leq 16 \\ \phi &= 2\pi f t \end{aligned} \tag{1}$$

where ϕ is the phase of the locomotion cycle, f its frequency, t the time, A_i the amplitude of the i-th joint and ψ_i the phase difference between the phase of the i-th joint and the phase of the locomotion cycle.

2) limbs: We control the limbs in the end-effector trajectory space, i.e. we define a trajectory for each foot which is followed precisely throughout the cycle. The reference frame for each pair of limbs (front and hind) is defined as the midpoint between shoulders or hips (Fig. 5). It is important to note that the x-axis of the reference frame is always parallel to the line of locomotion (the line that connects the centers of the front and hind limbs). The y-axis is on the vertical direction and the z-axis on the lateral. This means that the foot trajectory is independent from the oscillation amplitude of the trunk. A trajectory is defined by a set of three trigonometric equations, one for each axis. A point $\mathbf{p} = (x, y, z)$ of this trajectory is given by:

$$\begin{aligned} x &= A_x sin(\phi + \xi) + X \\ y &= \begin{cases} A_y cos(\phi + \xi) + Y & \text{if } cos(\phi + \xi) \leq 0 \\ Y & \text{else} \end{cases} \\ z &= \begin{cases} A_z cos(\phi + \xi) + Z & \text{if } cos(\phi + \xi) \leq 0 \\ Z & \text{else} \end{cases} \end{aligned} \tag{2}$$

where $A_{x,y,z}$ represent the amplitude of the movement at each axis and X, Y, Z the corresponding offsets. ϕ is, as before, the phase of the locomotion cycle and ξ the phase lag between the phase of the foot and ϕ. In other words, the foot follows a kind of semicircular trajectory. In stance phase, it follows a straight trajectory (of length $2A_x$), backwards, at constant offsets Y and Z from the reference frame of the limb. The offset X defines the front-back asymmetry of the stride around the shoulder/hip, i.e. positive X would retract the foot more than protract it. In swing phase the foot is cleared from the ground up to a height A_y and extended from the body at a distance up to $Z + A_z$. Thus, the above 6 variables are the ones to control the shape of a trajectory. After the definition of a foot's trajectory we use inverse kinematics to calculate the pitch, yaw and knee angles (θ_p,θ_y,θ_k) of the model. Given a point $\mathbf{p} = (x, y, z)$ on the trajectory and l_1, l_2 the lengths of the upper and foreleg respectively, it is possible to find analytical expressions for the three angles:

$$\begin{aligned} \theta_p &= atan2(z, y) - atan2(l_2 sin(\theta_k), \beta cos(\theta_y)) \\ \theta_y &= asin\left(\frac{x}{\beta}\right) \\ \theta_k &= \frac{asin\left(\frac{\alpha}{l_1}\right) + asin(\|\mathbf{p}\| - \alpha)}{l_2} - \pi \\ \alpha &= \frac{l_1^2 - l_2^2 + \|\mathbf{p}\|^2}{2\|\mathbf{p}\|} \\ \beta &= l_1 + l_2 cos(\theta_k) \end{aligned} \tag{3}$$

We control the duration of the stance phase over the cycle duration (duty factor), thus, the type of gait, with the follow-

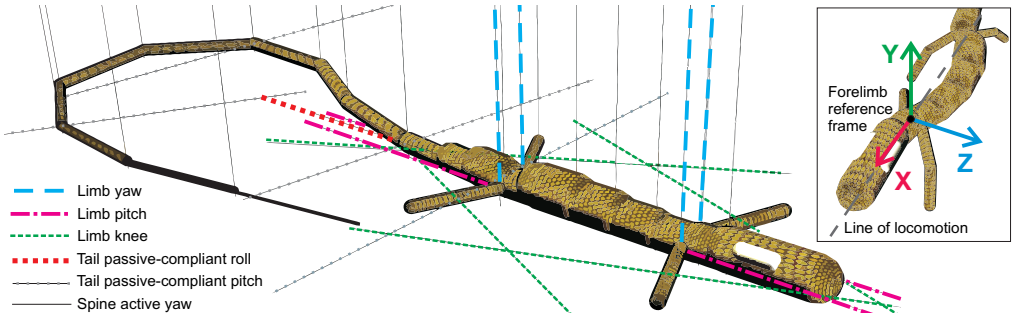

Fig. 5. The long-tailed lizard model. Definitions of the active and passive DoF denoted with different line styles and colors. (top right) Illustration of the line of locomotion and the reference frame of the forelimbs (the definition is similar for the hind limbs).

ing transfer function:

$$\phi_n = \begin{cases} \frac{\pi}{2\pi - D_f}\phi_p & \text{if } \phi_p \leq S_t \\ \frac{\pi}{D_f}(\phi_p - S_t) + \frac{\pi}{2} & \text{if } \phi_p \leq S_w \\ \frac{\pi}{2\pi - D_f}(\phi_p - S_w) + \frac{3\pi}{2} & \text{else} \end{cases} \quad (4)$$

$$S_t = \pi - \frac{D_f}{2}$$

$$S_w = \pi + \frac{D_f}{2}$$

where ϕ_p and ϕ_n correspond to the phase of the trajectory before and after the transformation based on the duty factor D_f which, in the equation, is expressed in radians. We will discuss more on the role of this parameter in section IV-B.

IV. SIMULATION EXPERIMENTS

A. Design of experiments

The simulated long-tailed lizard has a total of 64 control parameters. In order to systematically explore the behavior of the model we reduced this number to 10 based on some initial hypotheses.

To minimize the open parameters for the spine we defined one global variable for the amplitude of oscillation, A for the head and trunk joints and $A/2$ for the tail (eq. 1). We reduced the amplitude of the tail (with respect to the trunk) due to its length. Moreover, we hypothesize that while walking the animal uses only standing waves (and not traveling) which translates to $\psi = 0$ or $\psi = \pi$ in eq. 1. At the joints where the ψ changes value, the lateral direction of the standing wave changes and forms an S-shape instead of a C-shape. These points are the nodes of the standing wave. We defined three nodes in this model, two at the centers of the shoulders/hips of the forelimbs and hind limbs and one at the middle of the tail.

We also fixed the phase relationships between limbs themselves and limbs with body. From our prior knowledge from salamanders ([9]) we know that sprawling animals tend to begin the stance phase of a limb when the trunk is fully contracted at the opposite side in order to increase stride length. For our model, this means $\xi = 0$ for the right hind limb and the left forelimb. Moreover, in this study we focus on walking trot gaits where the contralateral limbs are in anti-phase, i.e. $\xi = \pi$ for the left hind limb and the right forelimb.

For the trajectories of the limbs two are the main hypotheses that reduced the number of open parameters; 1) symmetrical limbs have the same trajectories since the gait is symmetric and 2) the clearance of the feet from the ground, as soon as it is positive, does not affect the speed on even substrate.

To summarize, the parameters that we explore in this study are: 1) the amplitude of body oscillation, A, 2) the frequency, f, 3,4) the protraction-retraction of the forelimbs and hind limbs, A_x, 5) the distance of the shoulders from the ground, Y^{FL}, 6) the distance of the hips from the ground, Y^{HL}, 7,8) the lateral placement of the front and back feet from the line of locomotion, Z^{FL} and Z^{HL} respectively, 9) the offset of the protraction-retraction with respect to the hips, X_{HL} and 10) the duty factor D_f.

With the reduced number open parameters we performed systematic tests with small resolution for each variable in order to get a general view for the behavior of the model (this already led to a high number of experiments). For most of the parameters we used 3 instances except for the frequency for which we tested 6 different values in the range of the animal recordings. The table of experiments is shown in Table II. For each test we let the simulation run for 5 s which was enough time for the model to perform several cycles as the frequency was higher than 4 Hz. We then measured the forward speed as the distance traveled in the given time window.

B. Results

The best solutions from the simulation tests concerning forward speed as a function of the locomotion frequency were very similar to the animal data. This is particularly interesting for two main reasons: i) we only copied the morphometrics of the animal while the control was mostly free for optimization and ii) Sliding or locomotion instability may easily occur as long as the kinematics are not proper. Fig. 6 shows with a solid black line the performance of the model while, for convenience, the animal data are shown again here as scattered triangles. For each frequency, the individuals that achieved at least 90% of the best speed

TABLE II

TABLE OF EXPERIMENTS

Variable	Expr.	Low	Step	High	Unit	Resolution
A_{1-6}	A	0.1	0.05	0.2	rad	3
A_{7-16}	$A/2$	-	-	-	rad	1
$\psi_{1,2,7-11}$	0	-	-	-	rad	1
$\psi_{3-6,12-16}$	π	-	-	-	rad	1
f	-	4	1	9	Hz	6
A_x^{HL}	-	8	2	14	mm	4
A_y^{HL}	10	-	-	-	mm	1
A_z^{HL}	5	-	-	-	mm	1
X^{HL}	-	0	2	4	mm	3
Y^{HL}	-	6	2	10	mm	3
Z^{HL}	-	8	2	12	mm	3
A_x^{FL}	-	6	2	10	mm	3
A_y^{FL}	10	-	-	-	mm	1
A_z^{FL}	5	-	-	-	mm	1
X^{FL}	0	-	-	-	mm	1
Y^{FL}	-	8	2	12	mm	3
Z^{FL}	-	6	2	10	mm	3
$\xi^{RHL,LFL}$	0	-	-	-	rad	1
$\xi^{LHL,RFL}$	π	-	-	-	rad	1
D_f	-	40	10	60	%	3

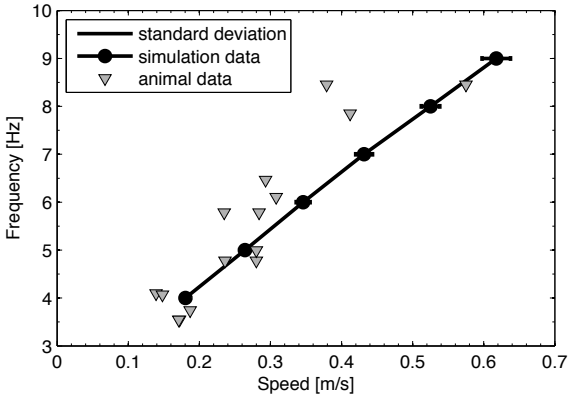

Fig. 6. Comparison between the frequency-speed response of the model (black line with circles) and the real animal (scattered triangles). The horizontal lines around the circles correspond to the standard deviation of the speed for the individuals that achieved at least 90% of the maximum speed at each frequency level.

were used to calculate the mean and standard deviation of the speed. As in the animal recordings, the long-tailed lizard model shows a linear relationship between speed and frequency, which is of course expected.

Although the real animals did not alter significantly the duty factor for different speed levels, the model showed a significant correlation. Fig. 7 shows with the black solid line the mean values of speed for the individuals that achieved the best speed for each value of duty factor. The real animal data is shown with triangles. The model shows a clear preference for shorter stance duration as speed increases. Note that the measurement of the duty factor in the real animal is expected to be slightly greater than the model's as in the first case the fingers extend the duration of the stance phase by staying on the ground for longer periods. However, the good match in the performance between the animal and the model might question the role of the fingers in propulsion

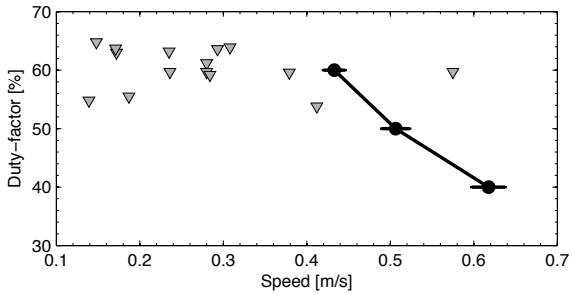

Fig. 7. Comparison between the duty factor-speed response of the model (black line with circles) and the real animal (scattered triangles). The horizontal lines around the circles correspond to the standard deviation of the speed for the individuals that achieved at least 90% of the maximum speed at each value of duty factor.

(we will not explore this hypothesis in this paper). Moreover, it is worth mentioning that the best results of the model take into account only the speed and ignore the cost in energy for employing flight phases. This might not be the case for the animals.

In Fig. 8 we present the results of the systematic tests for all the open parameters of the lizard model for the individuals that achieved at least 80% of the overall best speed ($N = 55$ individuals, speed range: 0.46 – 0.57 m/s). In other words we are looking into the preferences of the model for fast locomotion. For the explanation of the plots and the plot labels refer to the figure's caption.

The linear relationship between speed and frequency (Fig. 6) is reflected in the first plot of Fig. 8 where most of the fastest individuals used the maximum explored frequency, 9 Hz. Similarly, from the relationship of the duty factor with speed (Fig. 7), most of the individuals used the lowest possible value. A clear preference for the highest explored amplitude of the body's wave is shown by most of the 55 individuals. It might be interesting to extend the test boundaries for the three previous parameters in order to find their crest.

For the protraction length of the hind limbs (A_x^{HL}) most individuals are found at the 10 and 12 mm, with higher speeds achieved by the last one. This suggests that the longer the stride the better. Note that, for a leg of 15 mm total length the preferred stride length is close to the maximum physically possible. In the plot of the hind limbs' protraction-retraction offset (X^{HL}) we see that most individuals used more symmetric protraction and retraction lengths rather than pushing more backwards. It would be interesting to see if an offset towards the forward direction would yield better results, although that would be opposite to what we know from nature. Almost all the individuals used the lowest position for the hips (hind girdle, Y^{HL}). Note that lower values would yield the model's body to touch the ground making the 6 mm a physical limit. A wide placement of the hind feet (Z^{HL}) is preferred, but not the maximum explored value is used from most of the individuals as well as the fastest individual. This, most probably, is a result of the

limitation that the wide step is introducing to the step length.

Similar to the hind limbs, the forelimb's protraction-retraction length get the highest explored values of 10 mm. On the contrary, most of the fastest individuals preferred to keep the forefeet closer to the body-axis (Z^{FL}) yielding higher position for the shoulders (front girdle, Y^{FL}). Notice that, even though most of the individuals used a shoulders' height of 8 mm, the fastest of them used an even higher posture of 10 mm (observe the red dots in the plot of Y^{FL} which are sorted from low to high speed).

V. CONCLUSIONS AND FUTURE WORKS

We developed a model of the long-tailed lizard which is able to replicate the performance of the real animal in terms of speed without any prior knowledge of the specific animal's angular kinematics. Our simulation experiments suggested that an animal with such a morphology can run at high speed by: 1) increasing its frequency and body oscillation amplitude, 2) increase as much as possible the step length of the limbs, 3) reduce the stance duration and 4) keep a specific body posture where the hind limbs stay low and wide from the body-axis while the forelimbs stay higher and closer to the body axis. Surprisingly, the suggested posture is exactly the one that the long-tailed lizards use (Fig. 1). We have therefore shown that locomotion control and postural kinematics may well be coupled to morphology.

In this framework, in the future, we can explore several aspects of animal locomotion related to morphosis: i) postural kinematics for specific body types and ii) force and torque profiles using muscle-like actuation rather than simple position control.

VI. ACKNOWLEDGMENTS

This work was funded by the EU within the FP7 project Locomorph.

REFERENCES

[1] Aerts, P. and Van Damme, R. and Vanhooydonck, B. and Zaaf, A. and Herrel, A. (2000). Lizard Locomotion: How Morphology Meets Ecology. Netherlands Journal of Zoology 261, 0028-2960.

[2] Farley, C. T. and Ko, T. C. (1997). Mechanics of locomotion in lizards. Journal of Experimental Biology 200, 2177-2188.

[3] Martin, J. and Avery, R. A. (1998). Effects of tail loss on the movement patterns of the lizard, Psammodromus algirus. Functional Ecology 12, 794-802.

[4] Brown, R. M., Taylor, D. H. and Gist, D. H. (1995). Effect of caudal autotomy on locomotor performance of Wall Lizards (Podarcis muralis). Journal of Herpetology 29, 98-105.

[5] Lin, Z.-H. and Ji, X. (2005). Partial tail loss has no severe effects on energy stores and locomotor performance in a lacertid lizard, Takydromus septentrionalis. Journal of Comparative Physiology B: Biochemical, Systemic, and Environmental Physiology 175, 567-573.

[6] Reilly, S. M. and Delancey, M. J. (1997). Sprawling locomotion in the lizard Sceloporus clarkii: quantitative kinematics of a walking trot. J. Exp. Biol. 200, 753-765.

[7] Russell, A. P. and V. Bels. (2001). Biomechanics and kinematics of locomotion in lizards: Review, synthesis and prospectus. Comp. Biochem. Physiol. A 131:89112

[8] Hildebrand, H. (1966). Analysis of the symmetrical gaits of tetrapods.Folia Biotheoretica 4, 922.

[9] Kostas Karakasiliotis and A.J. Ijspeert (2009), "Analysis of the terrestial locomotion of a salamander robot", In Proceeding of IEEE IROS09, St. Louis, USA.

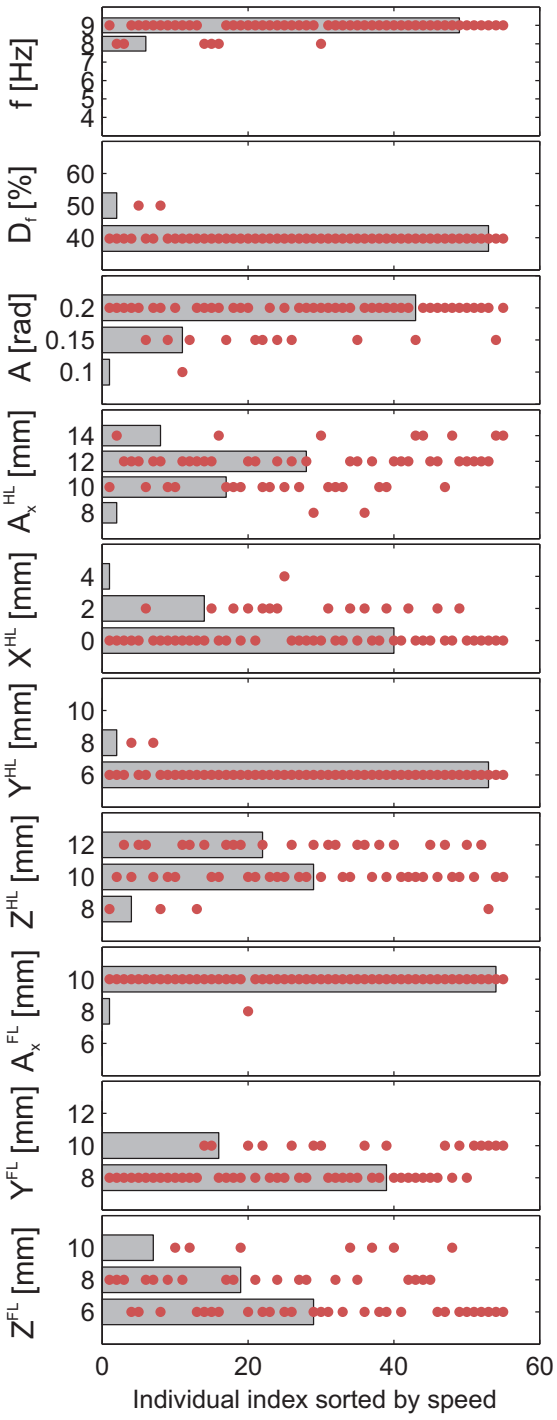

Fig. 8. Results from the systematic tests of the long-tailed lizard model for the individuals that achieved at least 80% of the best overall speed. In each plot the individual are shorted from the slowest to the fastest (1–55). The bars show the distribution of the preferred values of each parameter. The red dots denote which values each individual used. From top to bottom: frequency of locomotion (f), duty factor (D_f), amplitude of body's undulation (A), hind foot protraction length (A_x^{HL}), offset of the hind foot retraction (higher values yield further retraction backwards and, consequently, shorter protraction, X^{HL}), height of the hips (hind girdle) from the ground (Y^{HL}), lateral placement of the hind foot from the body-axis (Z^{HL}), forefoot protraction length (A_x^{FL}), height of the shoulders (front girdle) from the ground (Y^{FL}) and lateral placement of the forefoot from the body-axis (Z^{FL}).

D4.4.2.2

Studying morphosis with a simulated model of the long-tailed lizard *Takydromus sexlineatus*: tail amputation

Konstantinos Karakasiliotis

***Abstract*— Morphology is an important factor in locomotion. It may guide the control strategies that an animal or a robot uses for efficient locomotion. Based on our previous work for the modeling of the long-tailed lizard, in this paper we explore the effect of tail loss, a morphological feature that is particularly distinctive in this species. The main aim is to postulate and possibly predict the changes in the locomotor strategies and performance of an amputated long-tailed lizard. For our study we use optimization algorithms and we mainly focus on the results from the standard PSO (particle swarm optimization). Overall the effect of tail loss does not alter much the behavior of the model, both in terms of postural kinematics and speed performance. However some results show particular interest: first the amputated model uses half the power for achieving the same performance as the intact one, second the amputated model uses wider foot placement for the hind limbs and significantly smaller spinal oscillatory amplitudes. These results may predict that an amputated animal will experience stability problems at higher frequencies.**

I. INTRODUCTION

When it comes to fast, stable and adaptive locomotion, lizards are one of the best animal groups to study. Moreover, lizards display a wide range of morphological diversity and ecological adaptations, including the ability to locomote on a variety of substrates [1]. Lizard locomotor mechanics are remarkably similar to those of other legged animals [2] which suggests that similar locomotor strategies might be shared with other tetrapod groups. Understanding how specific morphological variations affect the locomotion strategies of animals may reveal the principles that connect morphology and control. Moreover, understanding the principles that connect morphology and control is particularly useful for robotics; it can guide the design of a robot for a particular task and provide a good basis for efficient and stable control.

Within the lizard taxon (Lacertilia), in the family of Lacertidae all members are relatively closely related. This increases the chances that observed morphological diversity within this family reflects functional diversity, and not phylogenetic diversity.

Within the Lacertidae, two species, the *Lacerta vivipara* and *Takydromus sexlineatus* have similar body size and they display a general "lizard" body shape, i.e. with not extremely strong (as is specialist runners) or underdeveloped (as in scincids) limbs. The specialist, *T. sexlineatus*, differs from the generalist *L. vivipara* mainly in one, clear, distinguishing feature: extreme tail elongation ([3] – [5]). This should facilitate interpretation of biomechanical comparisons between these species. *Lacerta* is the generalist reference, and a considerable amount of literature is available on general characteristics of lizard locomotion ([2], [6], [7]). Therefore, the main focus of our study is on *Takydromus* (Fig. 1) because it sports a clear case (tail elongation) of long-term morphosis. In the future, similar studies with *L. vivipara* could suggest potential differences in the locomotion control between these two species.

Konstantinos Karakasiliotis is with the École Polytechnique Fédérale de Lausanne (EPFL), Switzerland.

Fig. 1. Snapshot of the long-tailed lizard during the experiments.

In our previous study [8] we developed a simulated model of the long-tailed lizard able to replicate the speed-frequency response of the real animal. Our exploration was based on systematic tests for 10 control parameters on an intact model (i.e., with the same morphology and inertial characteristics of an intact animal). In this paper our goal is two-fold: i) first to deeper explore the performance of the intact lizard model using Particle Swarm Optimization and Viability Evolution. Optimization in a continuous space can provide better insight for the maximal performance of the model compared to the low resolution quantized systematic tests. ii) second to explore the effect of tail loss (intraspecific morphosis) on the locomotion control of the long-tailed lizard model.

II. THE LONG-TAILED LIZARD MODEL

A. Morphology and joints' topology

In [8] we developed a model of the long-tailed lizard in the ODE-based simulation platform Webots™. The segmentation, geometry and inertial properties of the model are based on the lizard's morphometric measurements. The spine of the lizard model is composed of 16 active degrees of freedom (DoF) with vertical axis of rotation and 5 passive compliant DoF of which 4 enable vertical movements and the last one rolling movements along the body-axis (Fig. 2). Each limb is composed of 3 active DoF and implemented as a pitch-yaw-knee manipulator. The pitch moves the limb vertically (adduction-abduction), the yaw, horizontally, back and forth (retraction-protraction) and the knee extends and retracts the foreleg.

For this study, additionally to the previous model, we used an amputated model. The tail was removed at a position close to the body (Amputation plane in Fig. 2). The tail should

not be removed from its connection to the trunk as in real animals some part of the tail is always needed for anatomical reasons (animal's vent).

B. Control

We use position control for all active DoF of the model with relatively high PID gains. This ensures that the defined postures and trajectories are respected, even in high frequencies.

1) Spine: The spine is controlled by a simple sine controller. The angle of each active DoF, θ, is given by:

$$\begin{aligned} \theta_i &= A_i sin(\phi + \psi_i), \quad 1 \leq i \leq 16 \\ \phi &= 2\pi f t \end{aligned} \tag{1}$$

where ϕ is the phase of the locomotion cycle, f its frequency, t the time, A_i the amplitude of the i-th joint and ψ_i the phase difference between the phase of the i-th joint and the phase of the locomotion cycle.

2) limbs: We control the limbs in the end-effector trajectory space, i.e., we define a trajectory for each foot which is followed precisely throughout the cycle. The reference frame for each pair of limbs (front and hind) is defined as the midpoint between shoulders or hips (Fig. 2). The x-axis of the reference frame is always parallel to the line of locomotion. The y-axis is on the vertical direction and the z-axis on the lateral. A trajectory is defined by a set of three trigonometric equations, one for each axis. A point $\mathbf{p} = (x, y, z)$ of this trajectory is given by:

$$\begin{aligned} x &= A_x sin(\phi + \xi) + X \\ y &= \begin{cases} A_y cos(\phi + \xi) + Y & \text{if } cos(\phi + \xi) \leq 0 \\ Y & \text{else} \end{cases} \\ z &= \begin{cases} A_z cos(\phi + \xi) + Z & \text{if } cos(\phi + \xi) \leq 0 \\ Z & \text{else} \end{cases} \end{aligned} \tag{2}$$

where $A_{x,y,z}$ represent the amplitude of the movement at each axis and X, Y, Z the corresponding offsets. ϕ is, as before, the phase of the locomotion cycle and ξ the phase lag between the phase of the foot and ϕ. In other words, the foot follows a kind of semicircular trajectory. In stance phase, it follows a straight trajectory (of length $2A_x$), backwards, at constant offsets Y and Z from the reference frame of the limb. The offset X defines the front-back asymmetry of the stride around the shoulder/hip, i.e. positive X would retract the foot more than protract it. In swing phase the foot is cleared from the ground up to a height A_y and extended from the body at a distance up to $Z + A_z$. Thus, the above 6 variables are the ones to control the shape of a trajectory. The calculation of the inverse kinematics for the limb joints are presented in [8]. The control variables will be further discussed in the optimization section.

III. Optimization

A. Optimization algorithms

We made extensive use of the standard PSO (particle swarm optimization) and we tested a new evolutionary algorithm, the Viability Evolution described in [9]. The particle swarm optimization is a very elegant, simple and fairly recent optimization algorithm [10], [11]. It is loosely based on the notion of swarm/flocking behavior. On the other hand, Viability Evolution (ViE) is an evolutionary algorithm based on iteratively reshaping constraints which define the viable space of solutions. The reproduction of individuals is not based on explicit fitness but rather on elimination according to the "environmental" constraints. ViE has proved to preserve diversity and therefore explore more solutions, however, in terms of implementation, contrary to PSO, it cannot be parallelized, demanding more (real) time for it to converge.

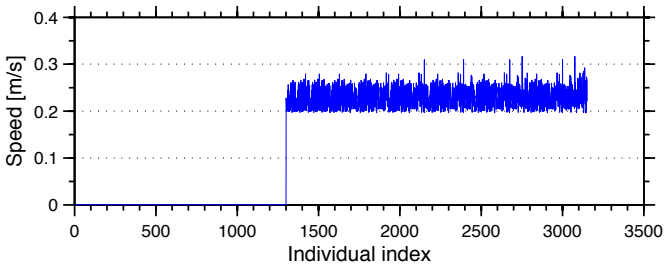

Fig. 3. Example of the ViE performance. The plot shows the evolved speed. The expected speed was around 0.6 m/s while the algorithm found much slower solutions (at the given number of individuals).

In our preliminary analysis[1] we found that ViE may not be very well suited for the lizard's optimization landscape. The landscape can be "flat" for several individuals and iterations mainly because of the small ranges in which the inverse kinematics of the limbs can find a valid solution (see Design of Experiments for details on the optimized parameters). This probably caused the ViE algorithm to be either very slow (in terms of convergence) or to oscillate around a suboptimal solution (compared to the expected one from the systematic tests). An example of the ViE output is shown in Fig. 3. In the figure, the speed of all individual is much slower than the expected one (see Results section).

B. Design of experiments

The simulated long-tailed lizard has a total of 64 control parameters. In our previous study we reduced this number to 11 based on several hypotheses. We used the same parameters both for the intact lizard model and the amputated one. Those parameters are: 1) the amplitude of body oscillation, A, 2) the frequency, f, 3,4) the protraction-retraction range of the forelimbs and hind limbs, A_x, 5) the distance of the shoulders from the ground, Y^{FL}, 6) the distance of the hips from the ground, Y^{HL}, 7,8) the lateral placement of the front and back feet from the line of locomotion, Z^{FL} and Z^{HL} respectively, 9,10) the offset of the protraction-retraction oscillation with respect to the hips and shoulders, X_{HL} and X_{FL} and 11) the duty factor D_f (ratio of stance duration over the locomotor cycle duration). The selected ranges for each variable are shown in Table I. Note that the frequency was not used as an open parameter for the

[1]We were able to run only a single experiment using ViE and therefore not explored several possible configurations of the algorithm.

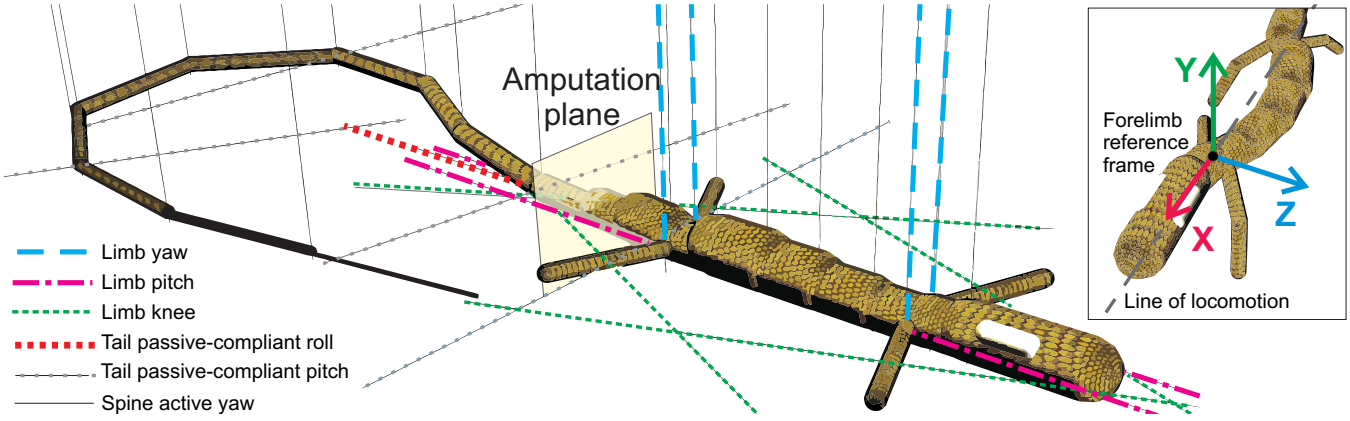

Fig. 2. The long-tailed lizard model. Definitions of the active and passive DoF denoted with different line styles and colors. (top right) Illustration of the line of locomotion and the reference frame of the forelimbs (the definition is similar for the hind limbs).

TABLE I
OPTIMIZATION PARAMETERS AND BOUNDARIES

Variable	Low	High	Unit
A	0	0.3	rad
f	4	9	Hz
D_f	20	80	%
A_x^{HL}	5	15	mm
X^{HL}	-5	5	mm
Y^{HL}	-5	5	mm
Z^{HL}	-5	5	mm
A_x^{FL}	5	15	mm
X^{FL}	-5	5	mm
Y^{FL}	-5	5	mm
Z^{FL}	-5	5	mm

individual optimization runs, but several optimizations were performed for different levels of frequency, every 1 Hz. In particular at least 5 optimization runs were performed for each frequency level. Whenever the results of similar optimization runs were not close to each other, up to 10 runs were performed in order to enhance the reliability of our conclusions.

For the fitness we measured only the speed of forward locomotion. However, a measure of the power consumption was recorded parallel to the fitness which we call effort. Effort is calculated as the sum of the squares of the joint/motor torques. The latter, although does not precisely give the power consumption (this would mean that a precise model of the motors is available), it gives a fairly good approximation of it.

In total, 68 different PSO optimizations were performed. Initial exploration for the number of iterations needed showed that 150 iterations for the intact model and 200 iteration for the amputated model were enough to ensure convergence. In both cases the number of particles was 50. This means that 7500 and 10000 individuals respectively were explored in each optimization run.

IV. RESULTS

A. *Frequency response of metrics*

In our previous work [8] we showed that the frequency response of the model, explored through systematic tests, was surprisingly close to the real data. For convenience those data are shown also here in Fig. 4. The black line with diamonds shows the results from the systematic tests and the real animal data are shown with green circles.

Interestingly, the optimization process, for the intact lizard model (blue squares), found a much faster solution for all the frequency levels. This suggests that relatively small changes in the coordination of the different DoF of the model may alter significantly its speed. The difference between the real data and the optimal speed achieved by the model may also suggest that the speed is not the only metric that animals account for (energy efficiency could be a second). Moreover, the mean optimal speeds of the amputated lizard model (red triangles) are almost identical, in most cases, with the intact's. The latter might not be very surprising as the main propulsion comes from the limbs and the bending of the trunk while the optimization process does not take into account the energy needed to achieve the same goal. Indeed, a plot of the effort of the two models for their optimal speed per frequency level shows that the amputated model is twice as efficient (Fig. 5).

The above results show that a more sophisticated fitness function, e.g. efficiency, could give results closer to the ones recorded from the animal in future experiments. A second observation that would demand further exploration is the effort-frequency response of the intact lizard model (blue squares; Fig. 5). Contrary to the effort response of the amputated model, which is linear, the intact model seems to use approximately the same effort for frequencies higher than 6 Hz, although its speed increases (blue squares; Fig. 4). This might mean that the model exploits the passive components of its joints, e.g. all the passive DoF in the tail (which are not present in the amputated model), and the compliant ground contact model.

The evolution of the best individuals for each iteration of

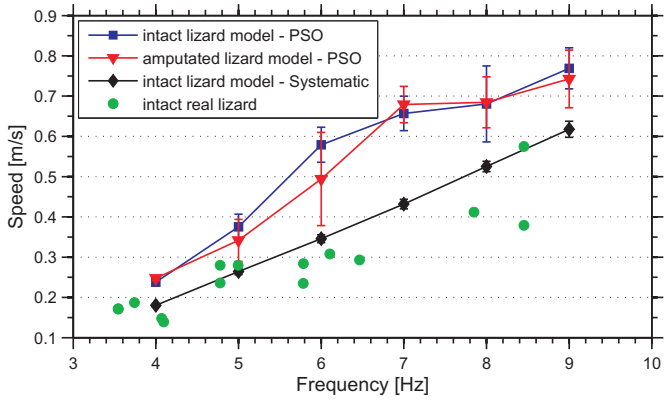

Fig. 4. Speed-frequency responses of the intact model using PSO (blue squares), the amputated model using PSO (red tringles), the intact model using systematic tests (black diamonds; data from [8]) and real animals (green circles; data from [8]).

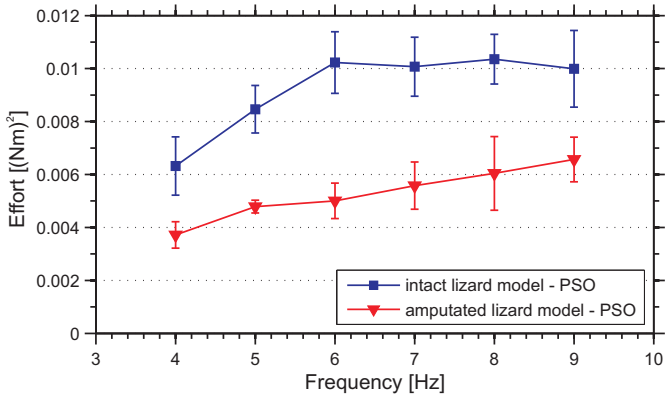

Fig. 5. Effort-frequency responses of the fastest intact model using PSO (blue squares) and the fastest amputated model using PSO (red tringles).

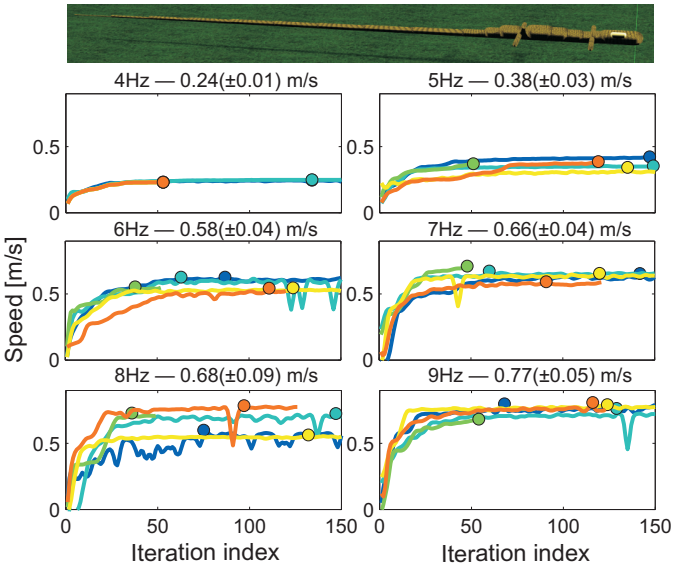

Fig. 6. Optimization process of the intact long-tailed lizard model. Evolution of the best individual for all the iterations of different optimization runs (different colored curves) for the different levels of frequencies (different plots). The colored circles denote the best individual for each run. The title of each plot gives the mean and standard deviation of the best individuals.

the different optimizations for the intact and the amputated model is shown in Fig. 6 and 7 respectively. Two observations can be made from the two figures: i) The majority of the optimization runs converged to a similar solution and ii) the majority of the optimizations converged to a solution close to their best in less than 50 iterations. The two observations show that the PSO works robustly and fast for the current problem.

B. Analysis of optimized control parameters

That the speed seems to have converged after the 50^{th} iteration for most of the optimization runs, it should not necessarily mean that the combination of the 10 control parameters is the same. A deeper analysis in the evolution of each parameter along the iterations of different optimizations showed that in our case similar values are used among best individuals (i.e. all the parameters followed a straight line after almost the 50^{th} iteration; Fig. 8 and 9). Some variability may also appear between different optimization runs of same parameters, i.e. different optimization runs may converge to the same speed but with different control parameters. Very few cases however show such a significant variability in our experiments with the majority of the parameters converging at similar values.

The optimized control parameters of the intact and the amputated models are more clearly shown in Fig. 10. For each frequency level, the parameters of the best individual of each optimization were selected for the calculation of the mean and standard deviation of each single parameter. The blue circles correspond to the values used by the intact model while the red triangles by the amputated.

From our previous systematic tests [8] we suggested that the optimal posture for a model with the morphology of the intact long-tailed lizard is the following: i) The hips should be kept close to the ground and the hind feet far from the body-axis (laterally) and ii) The shoulders should be higher than the hips and the front feet close to the body-axis. The results from the optimization of the intact model show the same pattern (Fig. 10; blue lines and circles). In particular, the hip height (Fig. 10E) is always slightly lower than the one of the shoulders (Fig. 10F). Also, the hind feet (Fig. 10G) are placed in a wider posture than the front ones (Fig. 10H) for the majority of the cases.

In terms of control, the intact model (blue circles in Fig. 10) shows a quite variable behavior for the spinal oscillatory amplitude (Fig. 10I) with the lowest bending found at the two extremes of the frequency range and the highest inbetween. The duty factor (Fig. 10J), more obviously in low frequencies, shows a slight tension to decrease which means that the model goes from walking to running gaits as frequency increases. Although the retraction range (how much they move back and forth) of the hind limbs is not significantly variable, the forelimbs seem to slightly decrease their range as the frequency increases. The latter could mean

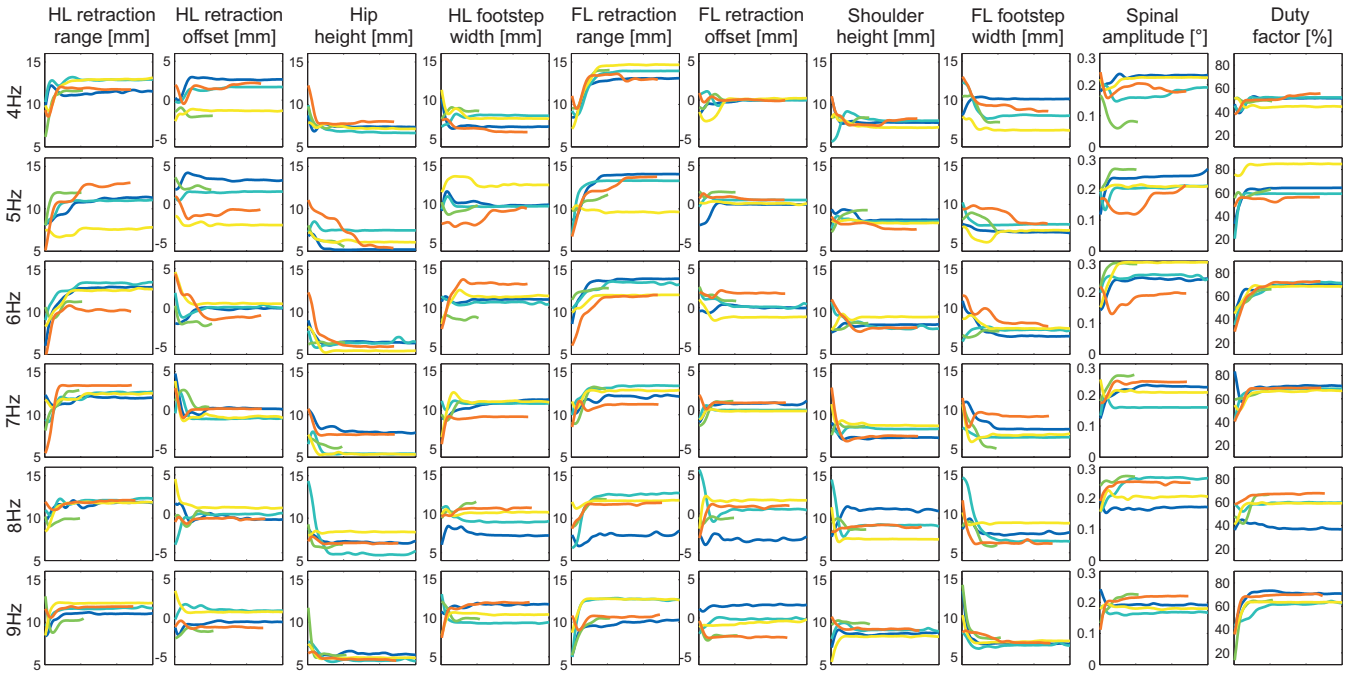

Fig. 8. Evolution of each control parameter of the intact long-tailed lizard model with respect to the iteration number for all optimization runs.

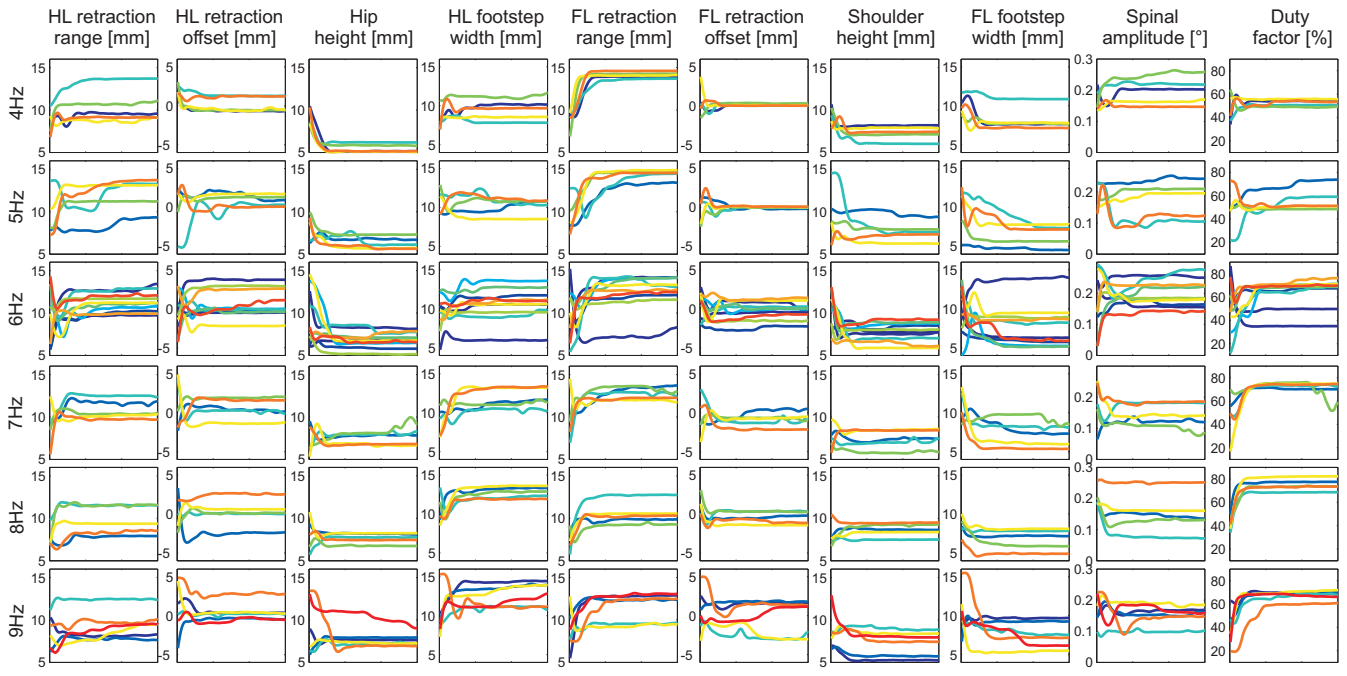

Fig. 9. Evolution of each control parameter of the amputated long-tailed lizard model with respect to the iteration number for all optimization runs.

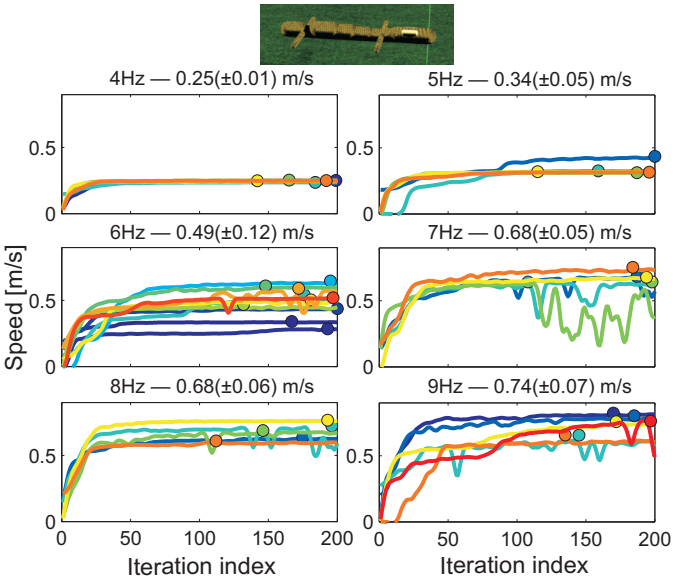

Fig. 7. Optimization process of the amputated long-tailed lizard model. Evolution of the best individual for all the iterations of different optimization runs (different colored curves) for the different levels of frequencies (different plots). The colored circles denote the best individual for each run. The title of each plot gives the mean and standard deviation of the best individuals. Note that for some frequencies (e.g. 6 Hz) more runs were needed because of the spread of the converged results.

that the role of the forelimbs slightly decays as the frequency and thus speed increases. That the retraction offset of both the hind and forelimbs remains close to zero, it means that the model prefers to use symmetric protraction and retraction around the hips and shoulders.

Overall, the effect of tail loss did not seem to alter much the behavior of the long-tailed lizard model (red triangles; Fig. 10). The trend of each variable with respect to the frequency remained the same or very similar. Only a few parameters were affected. The amplitude of spine undulations was significantly reduced for frequencies higher than 4 Hz (Fig. 10I). The lateral placement of the hind feet was also increased for most of the frequencies (Fig. 10G) while the front feet showed the same exact values as for the intact model (Fig. 10H). The two latter observations may suggest that the tail loss reduces stability as smaller amplitudes and wider hind feet placement yield more stable gaits. Another small change appears at the relative heights of the hips and shoulders. The amputated model uses slightly more balanced (parallel to the ground) posture for the trunk (Fig. 10E and F). This might be related to the reduced weight at the model's hips due to the tail loss. Finally, the retraction range of the hind limbs is reduced in the amputated model (Fig. 10A) probably because the propulsion from the front feet is enough to pull the model forward. The additional friction induced by the contact of the tail with the ground and due to the higher normal forces at the hind limbs may increase the importance of the hind limbs' retraction range.

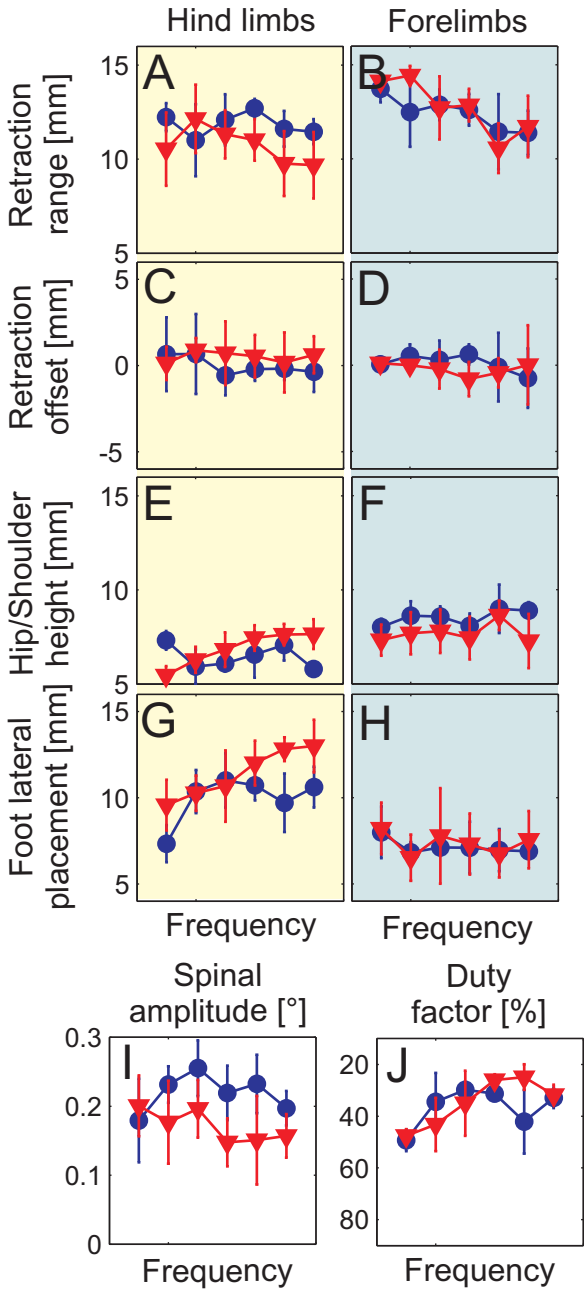

Fig. 10. Analysis of the optimized parameters. Each plot shows the mean and standard deviation (error bars) of a single optimized parameter of the intact long-tailed lizard model (blue squares) and the amputated model (red triangles) as a function of the different frequency levels (4 – 9 Hz). The mean values are calculated from several optimization runs of the same frequency. (A, B) Protraction-retraction range of the hind limbs and forelimbs, A_x^{HL} and A_x^{FL}, (C, D) Offset of the protraction-retraction oscillation with respect to the hips and shoulders, X_{HL} and X_{FL}, (E, F) Height of the hips/shoulders from the ground, Y^{HL}/Y^{FL}, (G, H) Lateral placement of the hind and front feet from the line of locomotion, Z^{HL} and Z^{FL} respectively, (I) Amplitude of body oscillation, A, (J) Duty factor D_f.

V. CONCLUSIONS AND FUTURE WORKS

The analysis of the long-tailed lizard's locomotion through optimization has confirmed our observations related to the animal's posture from previous systematic tests. However, the optimization using speed as a fitness failed to reproduce the animal data. Our hypothesis is that animals account for efficiency and therefore more sophisticated fitness functions should be explored in the future. In terms of morphosis, we explored the effect of tail loss by comparing the intact with the amputated model over the same set of parameters. That the overall behavior of the model did not change significantly it should not be unexpected as the tail does not, potentially, play a big role in ground propulsion. However, two interesting hypotheses and possibly predictions can be made for the walking behavior of an amputated long-tailed lizard: 1) the animal could be more unstable and to compensate for this it would use a wider posture for the hind feet and reduced body undulations. 2) it would use more level trunk postures (parallel to the ground) and the hind limbs would reduce their protraction-retraction range.

In the future it would be interesting to look into data from real amputated animals and evaluate our predictions. Moreover, apart from the more sophisticated fitness functions, other types of environments should be explored, e.g. slopped terrain and different ground friction coefficients.

VI. ACKNOWLEDGMENTS

The research leading to these results has received funding from the European Community's Seventh Framework Programme FP7/2007-2013 - Future Emerging Technologies, Embodied Intelligence, under grant agreement no. 231688. The author acknowledges also the help of Andrea Maesani for his help for setting up the AEON framework.

REFERENCES

[1] Aerts, P. and Van Damme, R. and Vanhooydonck, B. and Zaaf, A. and Herrel, A. (2000). Lizard Locomotion: How Morphology Meets Ecology. Netherlands Journal of Zoology 261, 0028-2960.

[2] Farley, C. T. and Ko, T. C. (1997). Mechanics of locomotion in lizards. Journal of Experimental Biology 200, 2177-2188.

[3] Martin, J. and Avery, R. A. (1998). Effects of tail loss on the movement patterns of the lizard, Psammodromus algirus. Functional Ecology 12, 794-802.

[4] Brown, R. M., Taylor, D. H. and Gist, D. H. (1995). Effect of caudal autotomy on locomotor performance of Wall Lizards (Podarcis muralis). Journal of Herpetology 29, 98-105.

[5] Lin, Z.-H. and Ji, X. (2005). Partial tail loss has no severe effects on energy stores and locomotor performance in a lacertid lizard, Takydromus septentrionalis. Journal of Comparative Physiology B: Biochemical, Systemic, and Environmental Physiology 175, 567-573.

[6] Reilly, S. M. and Delancey, M. J. (1997). Sprawling locomotion in the lizard Sceloporus clarkii: quantitative kinematics of a walking trot. J. Exp. Biol. 200, 753-765.

[7] Russell, A. P. and V. Bels. (2001). Biomechanics and kinematics of locomotion in lizards: Review, synthesis and prospectus. Comp. Biochem. Physiol. A 131:89112

[8] Karakasiliotis, K., D'Août, K., Aerts, P. and Ijspeert, A. J. (2012) Locomotion studies and modeling of the long-tailed lizard Takydromus sexlineatus. Accepted for publication in the proceedings of the Int. Conf. on Biomedical Robotics and Biomechatronics, Roma, Italy.

[9] Maesani, A., Fernando, P. R. and Floreano D. (2012) Artificial evolution by means of eliminations and environmental changes. Under preparation.

[10] Kennedy, J. and Eberhart, R. (1995). Particle swarm optimizationParticle swarm optimization. (4, 1942-1948 vol.4).

[11] Clerc, M. and Kennedy, J. (2002). The particle swarm - explosion, stability, and convergence in a multidimensional complex spaceThe particle swarm - explosion, stability, and convergence in a multidimensional complex space. Evolutionary Computation, IEEE Transactions on6158-73.

[12] Hildebrand, H. (1966). Analysis of the symmetrical gaits of tetrapods.Folia Biotheoretica 4, 922.

[13] Kostas Karakasiliotis and A.J. Ijspeert (2009), "Analysis of the terrestial locomotion of a salamander robot", In Proceeding of IEEE IROS09, St. Louis, USA.

D4.4.2.3

LocoMorph – Deliverable 4.4 part 2.3

Kinematic of locomotion in size-matched healthy and morphosed long-tailed lizards (*Takydromus sexlineatus*): effects of tail loss, incline and substrate type.

D'Août K, Karakasiliotis K, Ijspeert AL & Aerts P

Aim

Karakasiliotis *et al.*, 2012, have constructed a simulation model of locomotion in the long-tailed lizard (*Takydromus sexlineatus*). In order to further test this model, and ultimately better understand the effects of morphology and morphosis, experiments have been carried out on subjects of equal snout-vent length, but with an intact or a morphosed (mutilated) tail. Furthermore, two substrate slopes and two substrate types were tested.
Here we report the general findings on spatio-temporal gait variables.

Methods

Two individuals of similar (snout-vent) length were filmed in a custom-built arena: healthy (H) and mutilated tail (M). The arena has changeable substrates and inclines, and a mirror to allow synchronous recording of dorsal and lateral view.

- H: snout-vent length = 54mm, total body length = 335 mm
- M: snout-vent length = 56mm, total body length = 101 mm

Two slopes were tested: horizontal or level (L) and a slope of 23° (S), corresponding to the typical maximum slope animals could climb on a smooth substrate (paper).
Two substrates were tested: paper (P) and sandpaper of grain size 320 (S).
We attempted to record approximately ten trials in each condition if possible.
We used a RedLake MotionScope high-speed camera operating at 250 fps, spatial resolution was set at 1280*680 pixels. A Nikon 55mm micro lens was used, set at an aperture of f/11, and with shutter time shutter ranging from 1/500 to 1/2000 s under 1000 W halogen lighting.
Video footage was digitised using ImageJ, followed by standard calculation of spatio-temporal parameters in Excel and MatLab. Preferred speeds were compared using t tests. Because of speed effects on most gait variables, further analyses on the other variables were ANCOVA's with speed as a co-variate (and tests with the residuals being carried out at the overall average speed: 0.199 m/s).

Key findings & discussion

Preferred speed is significantly lower for the mutilated animal than for the healthy one, on both substrates. On paper, H trots at 0.23 ± 0.07 m/s and M at 0.15 ± 0.03 m/s ($p = 0.003$). On sandpaper, H trots at 0.26 ± 0.07 m/s and M (but only 2 data points) at 0.08 ± 0.00 m/s ($p = 0.001$).

Preferred speed does not differ between substrates in either the H or M animal ($p = 0.047$ and 0.184, respectively).

For the healthy individual, preferred speed is lower on the slope than on the level surface; this holds true for both substrates. On paper, speeds drops from 0.24 ± 0.07 to 0.16 ± 0.05 m/s ($p = 0.008$) and on sandpaper, speed drops somewhat less, from 0.26 ± 0.07 to 0.20 ± 0.10 m/s ($p = 0.045$).

Stride frequency differs significantly between most conditions (see Figure 1), except for the MLS condition (= mutilated, level, sandpaper) versus other conditions, but that is explained by the few (two) data points (i.e. not regressed on the graphs). For a given speed, the mutilated animal has a much higher stride frequency (blue and purple dots). For the healthy individual, the lines for the

equal substrates are closer to each other than the lines for equal slope, e.g. the substrate appears to have a larger impact here.

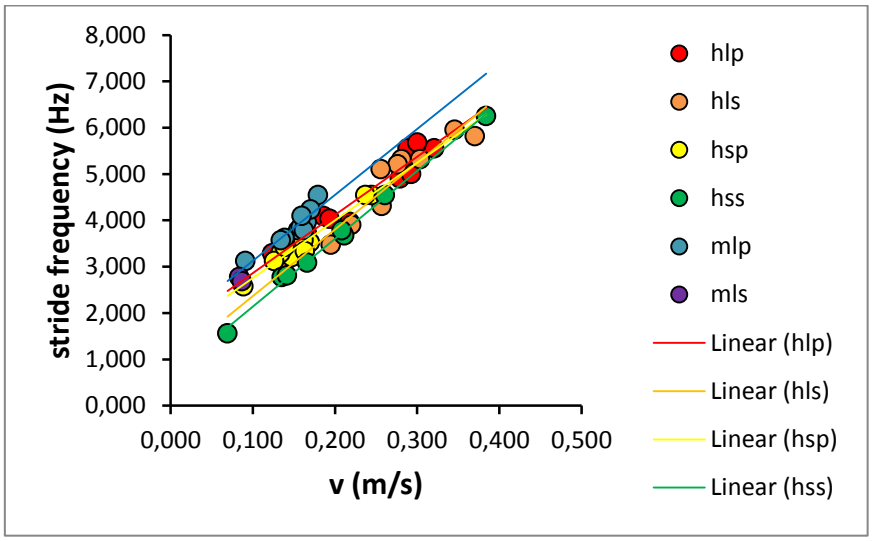

Figure 1

Stride length differs also (see Figure 2), and of course, shows an inverse pattern than frequency when looked on a speed-specific basis (i.e. stride lengths for the mutilated animal were low, although the mutilation was in the tail, not the limbs)

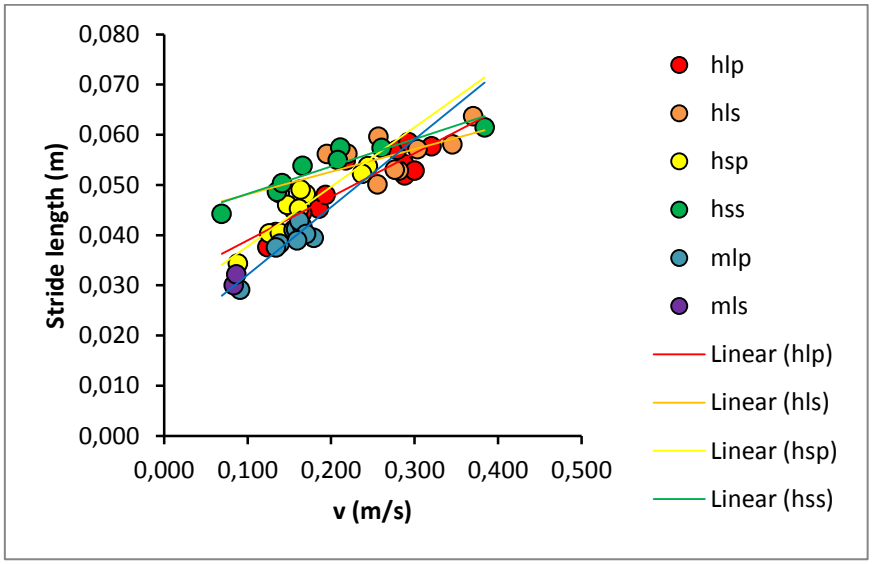

Figure 2

Hind limb duty factor decreases with speed (Figure 3), as expected, except for the mutilated animal but in this case, the speed range is small and R^2 is less than 1%, so we should ignore this. R^2 values for the other regressions are also not high (approx. 0.25 max.)

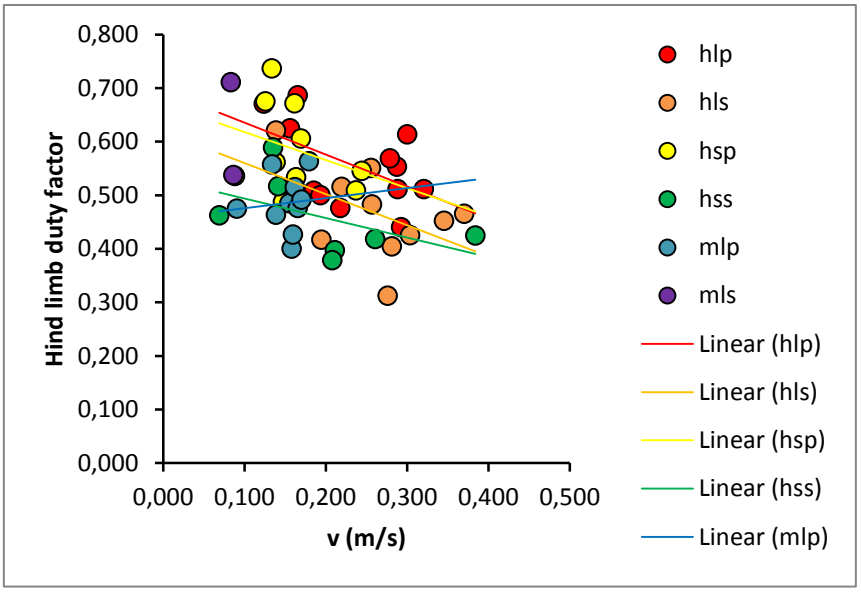

Figure 3

Forelimb duty factor, interestingly, remains more constant (see Figure 4). This goes well with the idea that the lizards are hind limb-driven. Overall, the forelimb also has a lower duty factor than the hind limb.

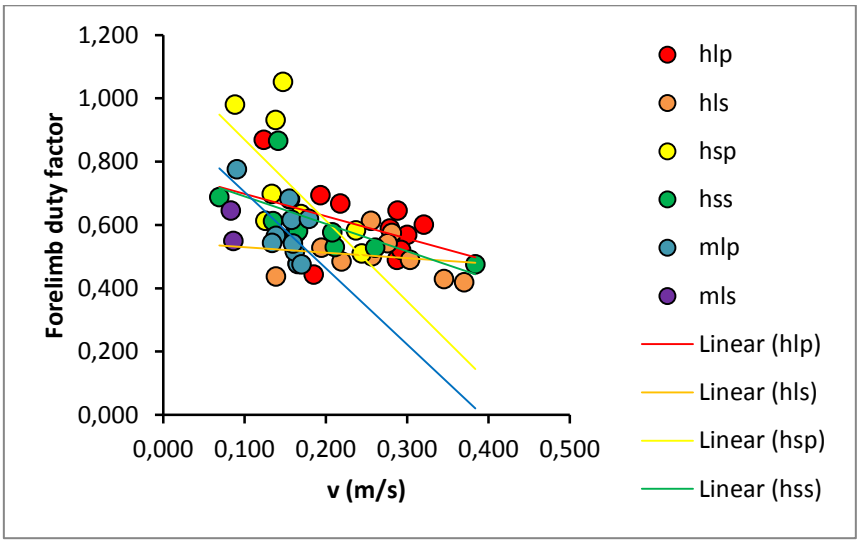

Figure 4

Laterality does not differ between conditions and is 0.424 on average (= relative delay of forelimb touchdown relative to ipsilateral hind limb touchdown, normalised for stride duration). This is reasonably close to a trot, where 0.5 is expected.

References

Karakasiliotis K, D'Août K, Aerts P and Ijspeert AJ (2012). Locomotion studies and modeling of the long-tailed lizard *takydromus sexlineatus*. *IEEE BIOROB2012*.

D4.4.2.4

LocoMorph – Deliverable 4.4 part 2.4

Kinematics in healthy and morphosed long-tailed lizards (*Takydromus sexlineatus*): comparison of a simulation model with experimental animal data.

D'Août K, Karakasiliotis K, Ijspeert AJ & Aerts P

Aim

Verification of the model output (see D4.4.2.2) with kinematics data collected in live long-tailed lizards (*Takydromus sexlineatus*).

Methods

Two individuals of similar (snout-vent) length were filmed in a custom-built arena: healthy (condition **H**) and morphosed (tail naturally autotomised; condition **M**). The arena has changeable substrates and inclines, and a mirror to allow synchronous recording of dorsal and lateral view.

- H: snout-vent length = 54mm, total body length = 335 mm
- M: snout-vent length = 56mm, total body length = 101 mm

Two slopes were tested: horizontal or level (L) and a slope of 23° (S), corresponding to the typical maximum slope animals could climb on a smooth substrate (paper).
Two substrates were tested: paper (P) and sandpaper of grain size 320 (S).
We attempted to record approximately ten trials in each condition if possible.
We used a RedLake MotionScope high-speed camera operating at 250 fps, spatial resolution was set at 1280*680 pixels. A Nikon 55mm micro lens was used, set at an aperture of f/11, and with shutter time shutter ranging from 1/500 to 1/2000 s under 1000 W halogen lighting.

Results were compared to the model output from Karakasiliotis et al (deliverable 4.4).
In all graphs, blue indicates the healthy, intact animal (H) and red indicates the morphosed animal (M), i.e. with tail mutilation.

Comparison of key model findings and experimental lizard data

Key findings from the model were (1) speed output for a given frequency is similar for H and M, (2) spinal amplitude is lower for M, (3) hind limb retraction range is smaller in M, (4) hip and shoulder height are more balanced, (5) hind foot placement is wider in M for most frequencies but not 5-6 Hz and (6) there is no effect of tail morphosis in forward speed.
We here directly address these findings by comparing them with data from the animal experiments.

1. Speed output for a given frequency is similar for H and M

The simulation study found that speed (the optimisation criterium) for a given frequency is overall similar between H and M (Figure 1), with a possible trend to higher frequencies for M at 6 Hz. Lizard experiments generally agree with this result, although the M subject did not perform at high frequencies (Figure 2; please note the different axis orientation in Figure 1 and Figure 2): the speed-frequency relationship (ANCOVA) is significantly different ($p=0.000$) between H and M, but the difference is small.

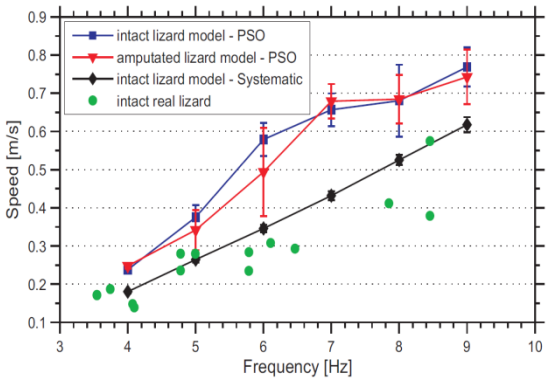

Figure 1 : speed-frequency relationship in simulated lizard locomotion (D4.4.2.2)

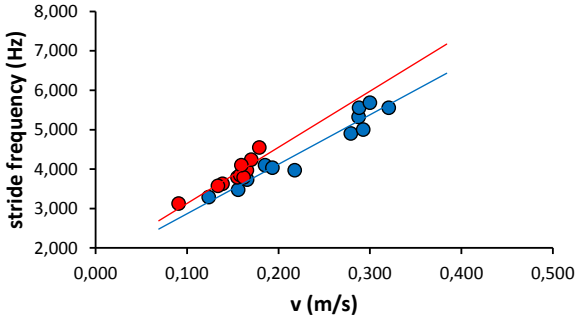

Figure 2 : speed-frequency relationship in lizards. Blue, healthy animal, red, morphosed animal.

2. Spinal amplitude is lower for M

Simulation output found smaller amplitudes at the spinal DOF's (i.e. smaller lateral wave amplitudes) for M. We observed a similar pattern in experimental lizards (Figure 3 : trunk posture at two extreme positions during a stride for H (top) and M (bottom).
Note the smaller wave amplitude for M.).

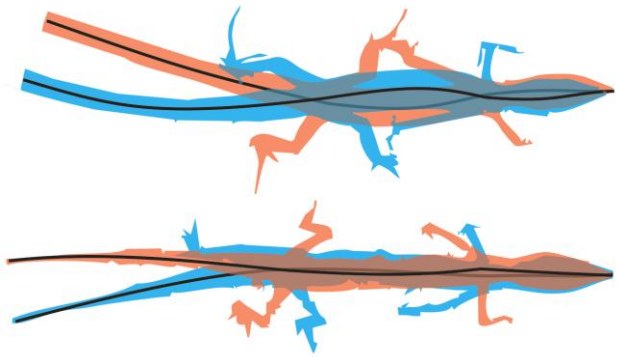

Figure 3 : trunk posture at two extreme positions during a stride for H (top) and M (bottom).
Note the smaller wave amplitude for M.

3. Hind limb retraction range is smaller in M

The simulation model found a smaller hind limb retraction range for M (Figure 4). This parameter corresponds to the distance travelled during one ground contact phase of the limb, i.e. step length. Experimental lizard data confirm this pattern (Figure 5) , however with step lengths being absolutely

approximately twice as large as in the model, i.e. 28,1 ± 3,1 mm for H and 18,9 ± 2,7 mm for M (ANCOVA p = 0.000).

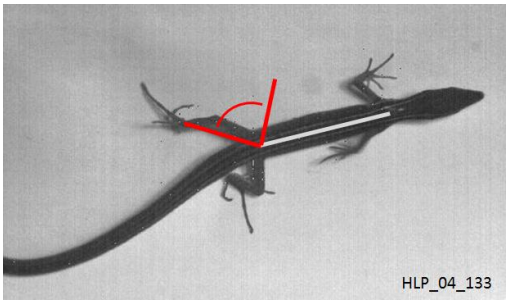

Figure 4 : screen shot taken at maximal hind limb retraction, with schematic illustration of hind limb retraction range.

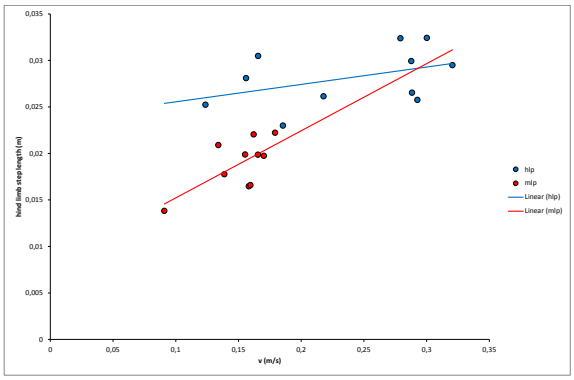

Figure 5 : the relationship between speed and hind limb retraction range,expressed as step length, in lizards.

4. Hip and shoulder height are more balanced

Simulations revealed a more “balanced” hip and shoulder height, in which the trunk inclined upwards for H and more horizontal for M. Lizard experiments (see Figure 6 for typical screen shots) show similar results. ANCOVA analyses confirm significantly (p = 0.001) more horizontal postures for M (Figure 7).

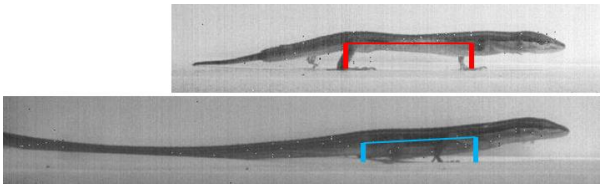

Figure 6 : lateral-view screen shots illustrating typical body postures in M (top) and H (bottom).

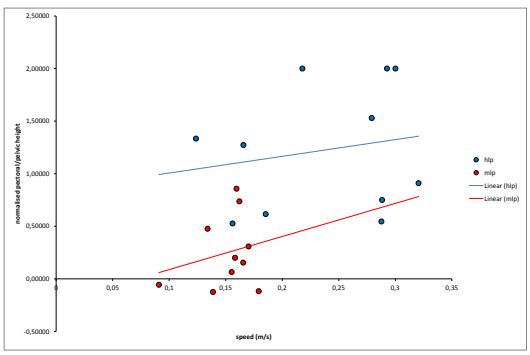

Figure 7 : the relationship between speed and relative heigth of the pectoral vs. the pelvic girdle. Because of digitisation accuracy/visibility, we measured the hight of the ventrum to the ground at the level of both girdles. The vertical axis

shows the difference between pectoral and pelvic height, normalised to average girdle height, so that a value of zero indicates a horizontal trunk posture and positive values indicate a relative lift of the shoulder.

5. Hind foot placement is wider in M for most frequencies but not 5-6 Hz

The simulation found wider (more lateral, Figure 8) hind limb foot placement for M, for the lowest and the highest frequencies and no difference at intermediate frequencies. Lizard data from low and intermediate frequencies show a significantly different ($p = 0.026$) foot placement, with M having slightly narrower placement (0.01013 ± 0.0006 m) than H (0.01113 ± 0.0012 m).

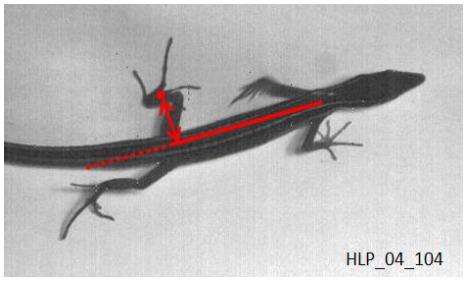

Figure 8 : screen shot illustrating the measurement taken, i.e. the distance from the center of the pelvic girdle to the pes.

6. Effect of tail morphosis in forward speed

In the simulation study, locomotor speed is optimised per condition (i.e. frequency), and it was found that H and M yielded similar speeds for similar frequencies. As discussed higher, in the lizards we found significant, but relatively small differences in the speed-frequency relationship (Figure 1 : speed-frequency relationship in simulated lizard locomotion (D4.4.2.2)). Other spatiotemporal variables deduced from animal experiments are similar for H and M (see Figure 9, and D4.4.2.3 for details).

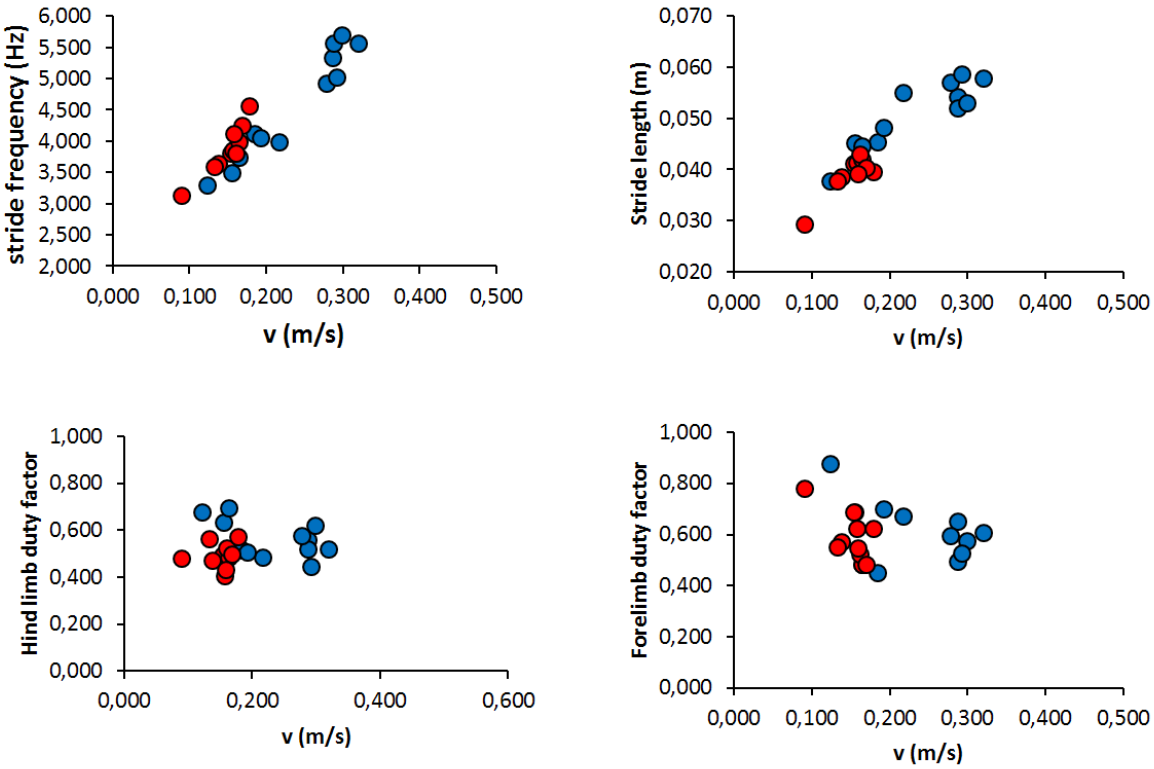

Figure 9 : frequency, stride length, and duty factors of fore- and hind limbsas a function of speed in the long-tailed lizard (see D4.4.2.3 for statistical analysis).

Conclusion

There is good correspondence between the simulation results using particle swarm optimisation (D4.4.2.2) and experimental data from lizards. The model is therefore valid and can be used to explore variation morphology and morphosis.